博 士 学 位 論 文
Doctoral Thesis

論文題目

Thesis Title

A Study on 20GHz-band DBF Transmitter Using Image Enhanced 1-Bit Bandpass Delta Sigma Modulator

東 北 大 学 大 学 院 工 学 研 究 科

Graduate School of Engineering,

TOHOKU UNIVERSITY

専攻/Department: Department of Communication Engineering

学籍番号/ ID No: B9TD9203

氏 名 /Name: Junhao Zhang (張 俊皓)

Table of Contents

List of Tables

List of Figures

Chapter 1

Introduction

1.1 Background

Since the 1800, the year that first wireless phone invented by Alexander Graham Bell and Charles Sumner Tainter occurred, the wireless communication technology has become a popular issue. After over 140-year development, now, the era of 5G is coming.

For 5G/B5G, the phantom cell [1] has been proposed and studied. The phantom cell is consisted of one macro cell operating in low frequency band, such as UHF band, whose communication distance is about 1 km and several small cells operating in high frequency, such as SHF and EHF band, whose communication distance is about several hundred meters. The control data (low speed) and user data (high speed) are transmitted by macro cell and small cell, respectively so that the high-speed and stable wireless communication can be achieved by phantom cell as shown in Figure 1.1. However, the higher attenuation in higher frequency band limits the capacity of 5G/B5G and becomes a problem. To solve it, the beamforming technology [2] has been proposed as shown in Figure 1.2. In the concept of beamforming, the directivity of antenna is improved by using multiple antennas (array antennas) and the sharper beam can be generated in high power level, which means the signal can be transmitted farther in high frequency band. Meanwhile, the direction of beam can be controlled by adjusting the phase difference of antenna element. Considering the moving terminals, the scan angle of beam should be as wide as possible.

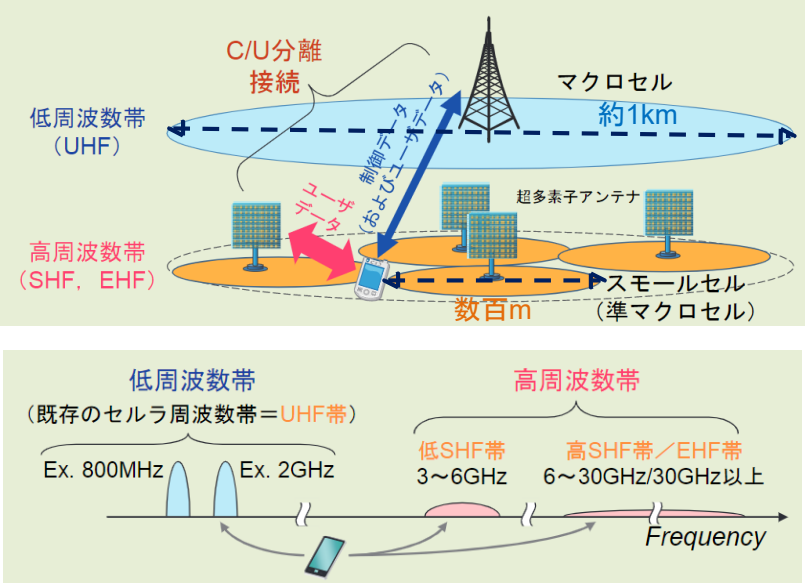

Figure 1.1: Phantom cell [1]

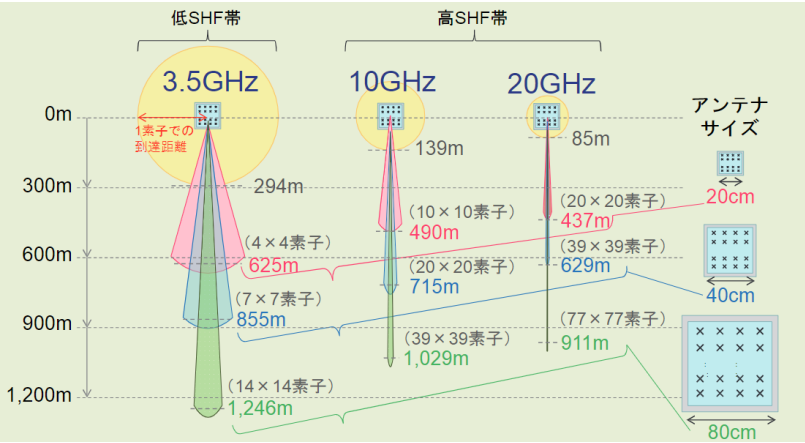

Figure 1.2: Beamforming technology [1]

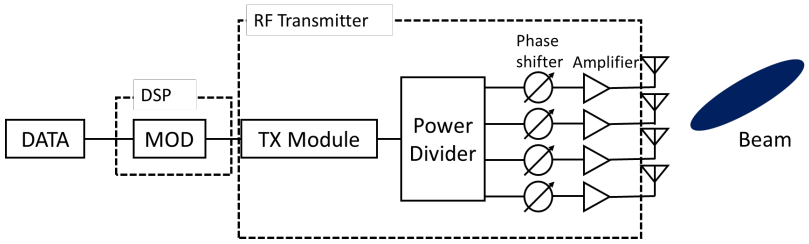

(a) ABF transmitter

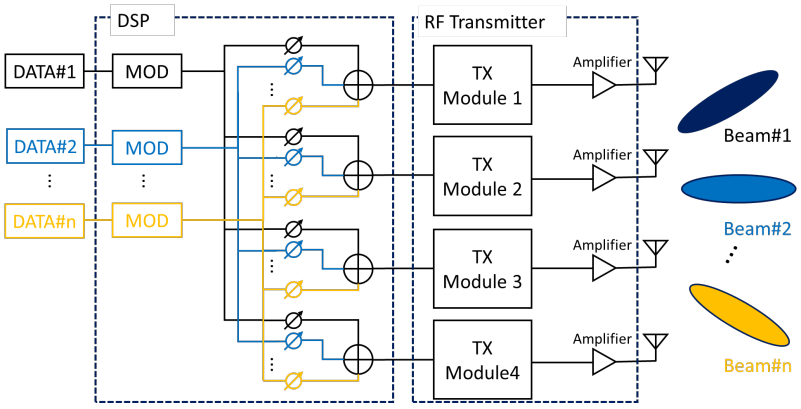

(b) DBF transmitter

Figure 1.3: Beamforming transmitter configuration

To implement the beamforming technology, there are two transmitter configurations as known as analog beamforming and digital beamforming [3]. As shown in Figure 1.3, in ABF, the phase shifter is implemented in RF transmitter (analog domain) so that only one transmitter module is needed. With a simple configuration, only one beam can be generated in one time slot, which is the cons of ABF that limits the capacity of whole system.

On the other hand, in DBF [4–6], the phase shifter is implemented in DSP (digital domain) so that each antenna element needs a transmitter module. Consequently, the DBF transmitter is much more complex than ABF transmitter. However, the DBF transmitter can generate multibeam for multiuser simultaneously which improves the capacity of whole communication system.

As a result, DBF has a great advantage on system capacity but the miniaturization of transmitter module is necessary for practical implementation.

An practical example of 64-element 28GHz-band DBF transmitter is presented in Figure 1.4 [7]. Obviously, configuration of multiple complex transmitter module limit the practical implementation of DBF transmitter especially in high frequency band at which the distance between each antenna element is very short.

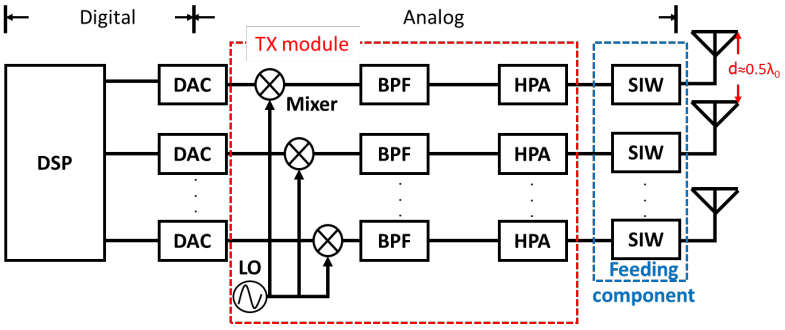

(a) Block diagram

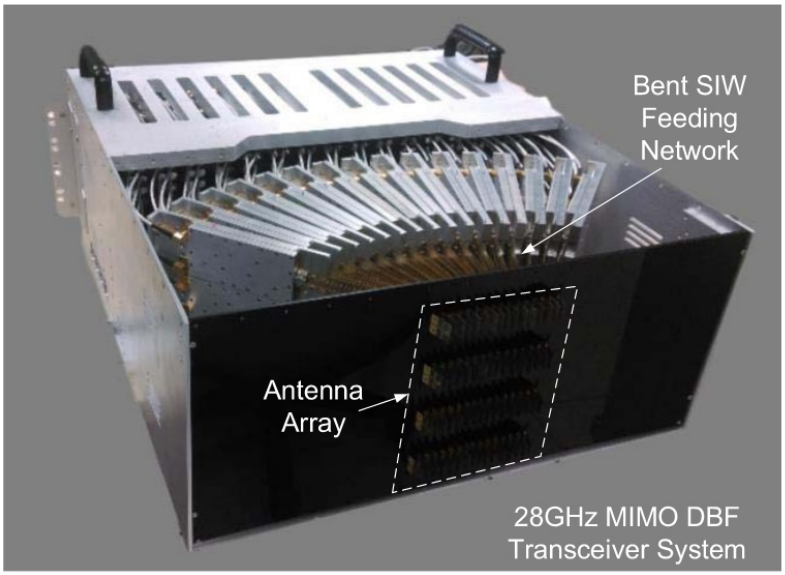

(b) Picture

Figure 1.4: Practical example of DBF transmitter [7]

Another problem of DBF transmitter in high frequency band is antenna. As shown in Figure 1.4, to connect the transmitter module with antenna, feeding components, such

as SIW, is necessary in previous research. To achieve the miniaturization of whole DBF transmitter, the integration between antenna and transmitter module is also a must.

1.2 Problems and Motivation

1.2.1 Direct Digital RF transmitter

To minimize the transmitter, digital RF technology [8–11] has been proposed. As shown in Figure 1.5, compared with the conventional transmitter, in digital RF transmitter, the RF signal is generated from DSP without up-converter (LO and mixer) so as to realize the miniaturization of transmitter. However, to generate RF signal at high frequency band, the high-speed DSP is necessary.

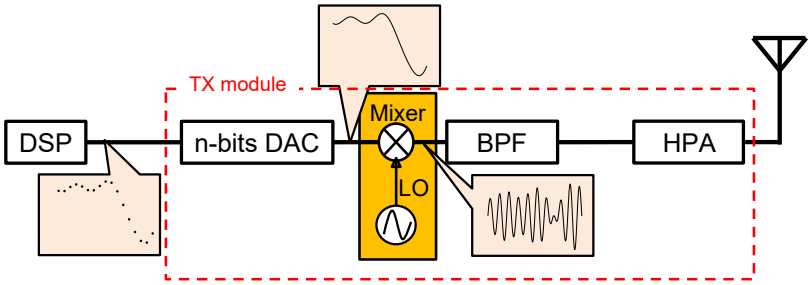

(a) Conventional transmmitter

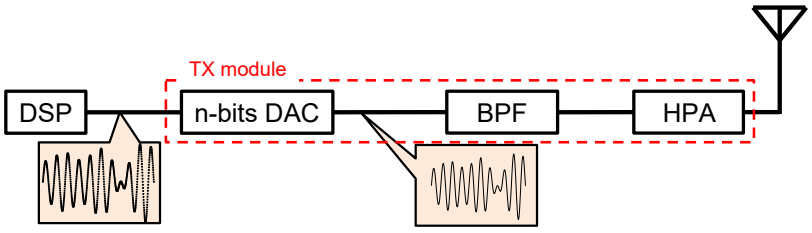

(b) Digital RF transmitter

Figure 1.5: Concept of digital RF

To improve the sampling rate (speed) of DSP, digital RF transmitter using 1-bit BP-DS modulator [12–16] has been proposed as shown in Figure 1.6.

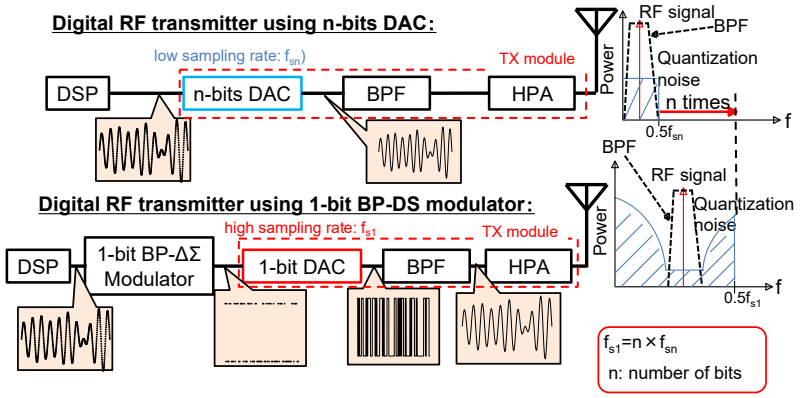

Figure 1.6: Digital RF transmitter using 1-bit BP-DS modulator

Compared with n-bits DAC [17–20], 1-bit DAC can improve the sampling rate by n times. Consequently, RF signal can be generated in higher frequency band. Moreover, because of the noise shaping characteristics of DS modulation, high dynamic range can be achieved. However, the maximum frequency of generated RF signal is half of sampling rate because of the Nyquist limit.

To overcome this limit, the direct digital RF transmitter [21–24] using the high order image component of 1-bit BP-DS modulated signal has been proposed. As it is known to all, in 1-bit signal, the fundamental component is folded to high Nyquist zone by every half of sampling rate. The folded components is known as image components. By using high order (beyond 2nd) image components, the RF signal can be generated at frequency band higher than sampling rate beyond Nyquist limit as shown in Figure 1.7. Since the upper limit of sampling rate has been improved to 6 GHz thanks to the development of CMOS technology [25], to generate RF signal at 20GHz-band, using high order (beyond 5th) image components is necessary.

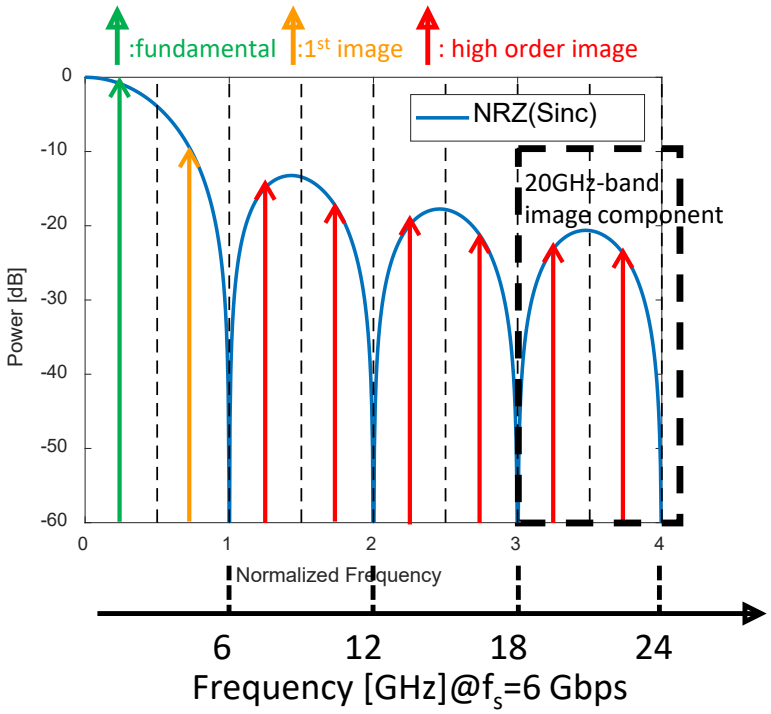

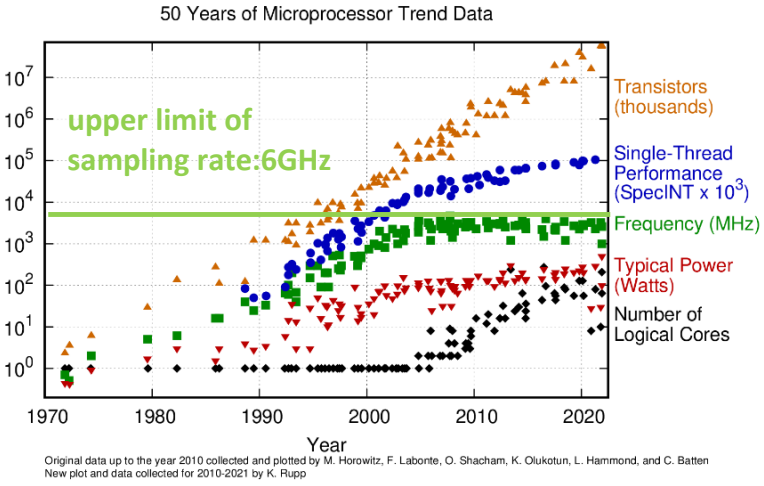

Figure 1.7: Direct digital RF transmitter [25]

The thorniest problem of direct digital RF transmitter is the attenuation of high order image components. There are two reasons for the attenuation in digital and analog domain, respectively, as shown in Figure 1.8. First, in digital domain, the high order image components of 1-bit BP-DS modulated signal generated by DSP in NRZ code attenuate in Sinc function [26,27]. For example, the 6th image components will suffer 20dB attenuation even in the condition of ideal waveform. The other one is frequency characteristics of 1-bit DAC which causes the degradation of rising/falling time of 1-bit signal. Consequently, the high order image components will attenuate severely furthermore [28–31]. The solution to this problem should also be addressed in both digital (signal generation) and analog (RF circuit) domain.

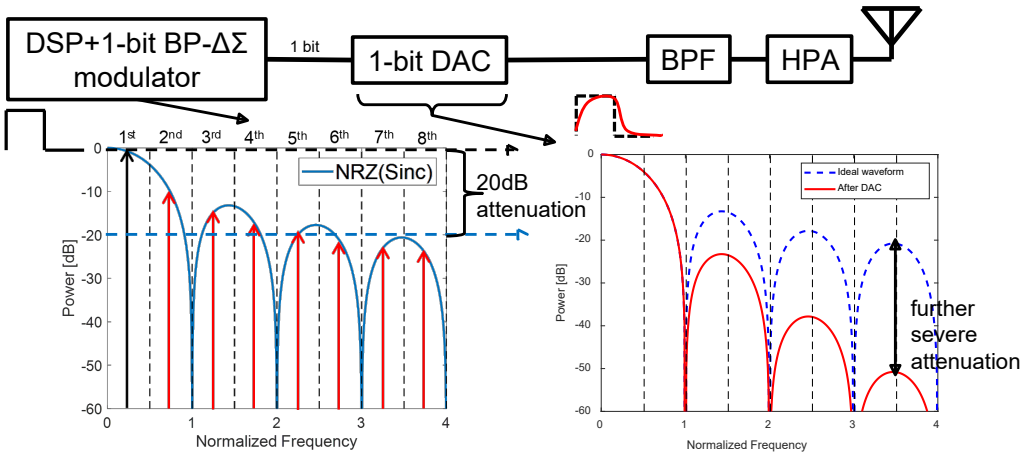

Figure 1.8: Problem of direct digital RF transmitter: attenuation of high order image components

1.2.2 Endfire Antenna

First and foremost, it should be declared that, in this thesis, the broadside and endfire antennas are classified by the beam direction to array antenna substrate

As shown in Figure 1.9, the beam generated by broadside antenna is vertical to the antenna substrate so that the coaxial connector is necessary to connect the antenna module to

transmitter module [32–34]. In contrast to that, the beam generated by endfire antenna [35–37] is horizontal to the antenna substrate so that the antenna module can be integrated with transmitter module directly on the same substrate. Obviously, the endfire antenna is a better choice for DBF transmitter.

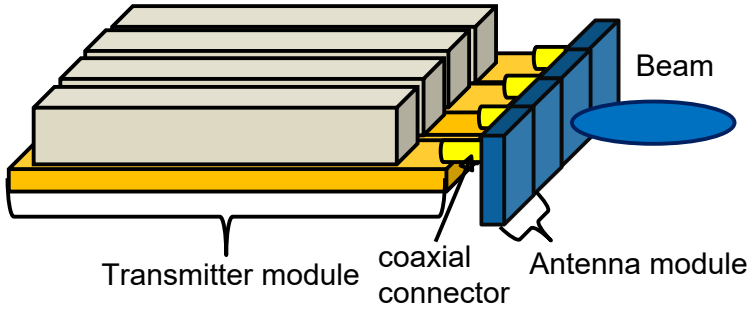

(a) Broadside antenna

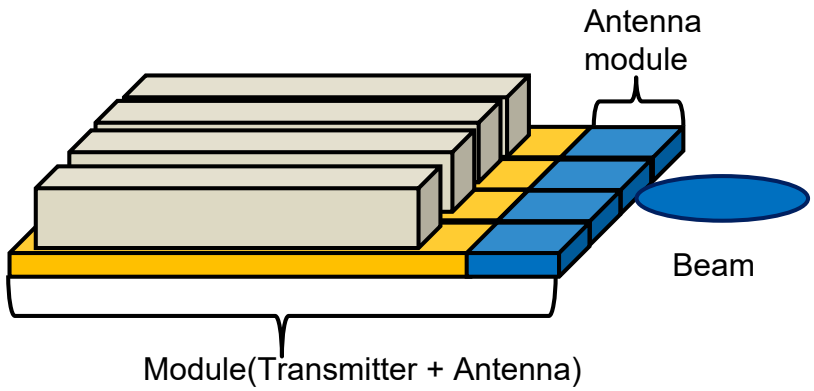

(b) Endfire antenna

Figure 1.9: Antenna configuration

The problem of using endfire antenna is its backlobe. As shown in Figure 1.10 [7], different from the broadside antenna, the backlobe power will be reflected by metal transmitter module to frontward which influence the mainlobe. Using shield can improve this phenomenon, but it will increase the complexity of transmitter which is not expected for miniaturization of transmitter. As a result, a low-backlobe endfire array antenna is necessary.

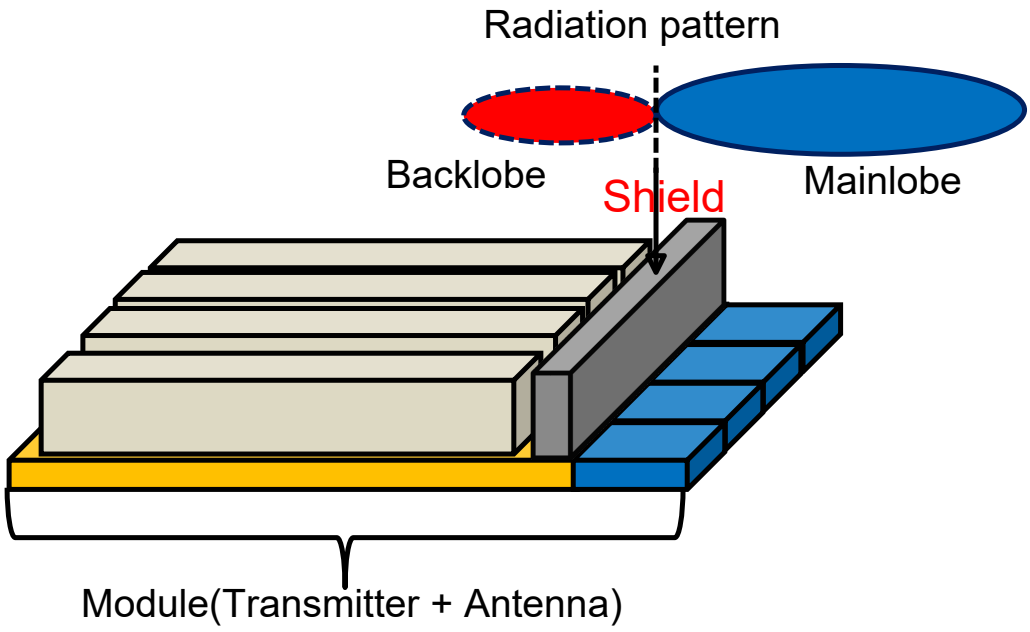

Figure 1.10: Problem of endfire: backlobe

1.3 Framework of Thesis

In this study, we propose an image enhancement technique using Manchester coding (digital domain) and RF tripler (analog domain). In addition, a low backlobe endfire Vivaldi array antenna whose front-to-back ratio (FBR) is beyond 20 dB to eliminate the backward leaked power is discussed.

The thesis is organized as followed and shown in Figure 1.11 Chapter 1 is introduction, which describes the background of the research. The requirements and challenges of 5G/B5G communication are introduced in this chapter.

Chapter 2 emphasizes on the image enhancement technique using Manchester coding in digital domain to improve the Sinc-function attenuation caused by NRZ coding. After illustrating the concept and principles by theoretical calculation, simulation and measurement are conducted to verify it. By setting the center frequency of 1-bit BP-DSM to quarter of sampling frequency, both the simulated and measured results have a good agreement

to theoretical calculation, which show that Manchester coding can improve the power of high order image components of 1-bit BP-DS modulated signal in the specific $(4n-1)^{th}$ and $(4n-2)^{th}$ Nyquist zone by 7.6 dB in digital domain compared to NRZ coding.

Chapter 3 emphasizes on the image enhancement technique using RF tripler in analog domain to improve the attenuation caused by the frequency characteristics of 1-bit DAC. Instead of using a high-speed 1-bit DAC based on inverter, RF tripler is proposed to regenerate the high order image components of 1-bit BP-DS modulated signal by its nonlinearity. 1-bit BP-DS modulated data in NRZ and Manchester code is used in theoretical calculation to verify the feasibility of the proposal. The simulation and measurement are also conducted. From the simulated and measured results, the regeneration of high order image components can be confirmed and the output power of regenerated 6^{th} image components by 1-bit BP-DS modulated signal in Manchester code is 13 dB higher than that in NRZ code, which is in accord with theoretical calculation.

Chapter 4 introduces a low-backlobe endfire Vivaldi array antenna. The backlobe is generated by the current on both edge sides. To reduce the current, slit is inserted on both edge sides. After the reduction of current is confirmed by using single slit, two-slit configuration is proposed to improve the FBR furthermore. In simulation, the FBR beyond 20 dB can be achieved both in antenna element and 4-element array antenna. In measurement, by putting a copper taper behind the array antenna as a reflector, the radiation pattern of mainlobe is almost invariant which means even if the backward leaked power is reflected, the mainlobe is not influenced.

Chapter 5 evaluates the fabricated 20GHz-band DBF transmitter using the proposed image enhancement technique and low-backlobe Vivaldi array antenna.

Chapter 6 is the conclusion.

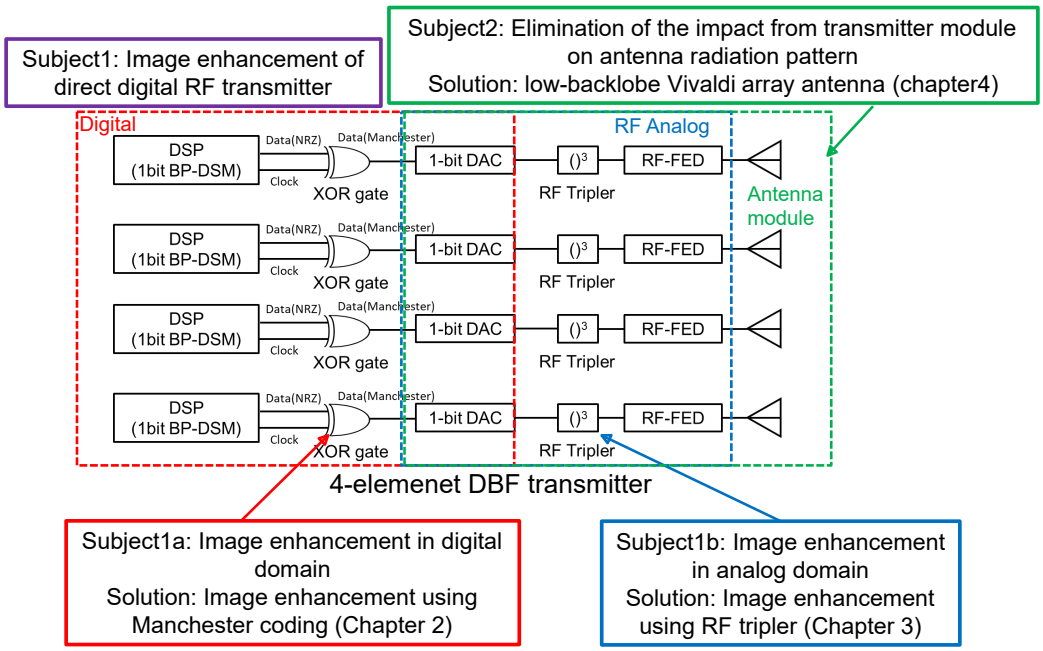

Figure 1.11: Framework of Thesis

Chapter 2

Image Enhancement Technique Using Manchester Coding in Digital Domain

In this chapter, instead of conventional NRZ coding, the Manchester coding is proposed to enhance the image components at specific Nyquist zone. The Manchester coding [38] can be easily implemented by using XOR gate on 1-bit data in NRZ code and synchronous clock [39]. So there will not be much more burden on DSP, such as complexity, power consumption and so on. It is proven by theoretical calculation, simulation and measurement that compared with NRZ coding, the image components of 1-bit BP-DS modulated signal at $(4n\text{-}1)^{th}$ and $(4n\text{-}2)^{th}$ Nyquist Zone can be enhanced by Manchester coding

2.1 NRZ and Manchester coding

The waveforms of NRZ and Manchester code are shown in Figure 2.1. Manchester code is a line code in which the encoding of each data bit is either low then high, or high then low, for equal time in one period. Manchester code can be easily implemented by using XOR gate on NRZ and synchronous clock signal. Compared to NRZ and RZ [40] code, in the Manchester code, the DC component is independent on 1-bit data and there is no clock leakage.

Figure 2.1: Waveforms of 1-bit data in NRZ and Manchester code

As shown in Figure 2.1, with a flip of waveform from low/high to high/low in one period, it is not difficult to image intuitively that the signals near the odd multiple numbers of sampling frequency are enhanced while signals away from the odd multiple numbers of sampling frequency are suppressed. However, the principle of this enhancement by using Manchester coding should be discussed more specificly by theoretical calculation, simulation and measurement, which will be presented in following section.

2.2 Theoretical Calculation of Power Spectral Density

1-bit BP-DS modulated signal can be regraded as a pseudo-random sequence so that its PSD can be calculated by Equation 2.2.1.

$$PSD(f) = f_s P(1-P)|G_1(f) - G_0(f)|^2 \tag{2.2.1}$$

f_s is sampling frequency (data rate) of 1-bit signal. P is the probability of data '0'. G_1 and G_0 are Fourier transform of g_1 and g_0, which are the waveforms of data '1' and '0', respectively.

2.2.1 NRZ coding

The waveforms and their mathematical expressions of 1-bit BP-DS modulated signal in NRZ code are shown in Figure 2.2.

1bit data: 1	1bit data: 0
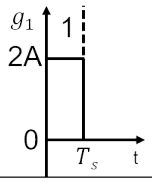 $g_1(t) = 2A,\ 0 < x \leq T_S$	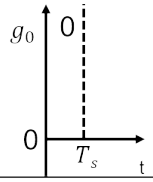 $g_0(t) = 0,\ 0 < x \leq T_S$

Figure 2.2: Waveforms and their mathematical expressions of 1-bit data in NRZ code

After calculation, the PSD of NRZ code can be expressed in Equation 2.2.2

$$PSD(f) = A^2 T_s \text{Sinc}^2(\pi f T_s) \tag{2.2.2}$$

A is the amplitude of 1-bit BP-DS modulated signal and T_s is period, which is the reciprocal of the sampling frequency, f_s. The calculation result is plotted in Figure 2.3 in the condition that both A and T_s are normalized.

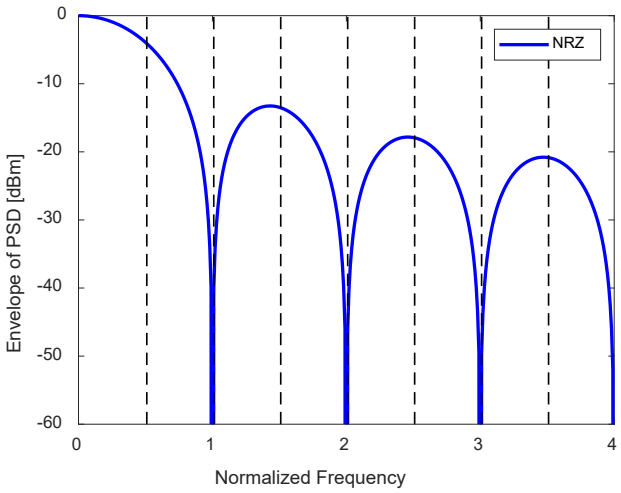

Figure 2.3: PSD of NRZ code

2.2.2 Manchester coding

The waveforms and their mathematical expressions of 1-bit BP-DS modulated signal in Manchester code are shown in Figure 2.4.

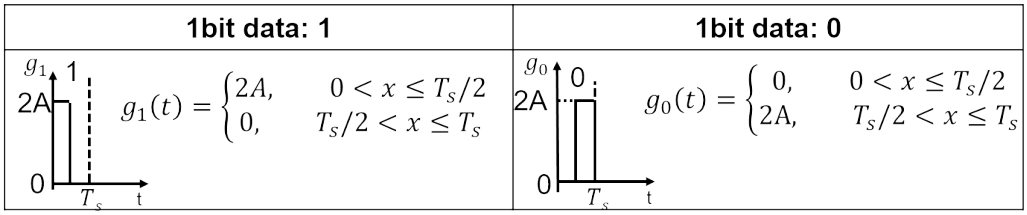

Figure 2.4: Waveforms and their mathematical expressions of 1-bit data in Manchester code

After calculation, the PSD of Manchester code can be expressed in Equation 2.2.3. The calculation result is also plotted in Figure 2.5 in the condition that both A and T_s are normalized.

$$PSD(f) = A^2 T_s \text{Sinc}^2(\pi f T_s/2)\sin^2(\pi f T_s/2) \tag{2.2.3}$$

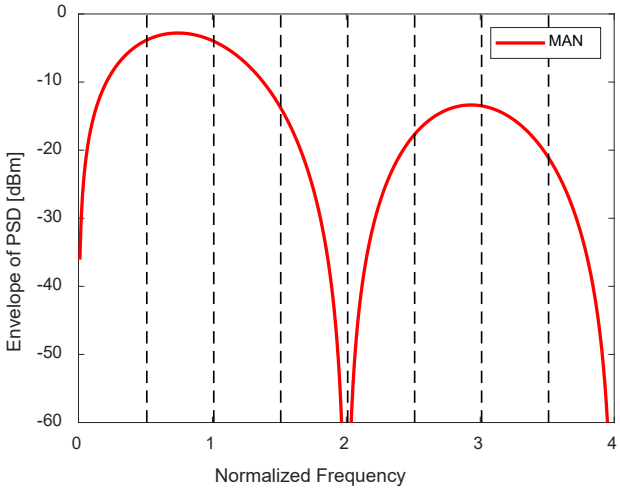

Figure 2.5: PSD of Manchester code

2.2.3 Comparison between the calculation results of NRZ and Manchester code

The exact value of the enhancement on PSD in Manchester coding is given by Equation 2.2.4.

$$\frac{PSD_{MAN}}{PSD_{NRZ}}(f) = \tan^2(\pi f T_s/2) \tag{2.2.4}$$

Let it be equal or larger than 1, which means the PSD of the Manchester code is higher than NRZ, the results are shown in Equation 2.2.5 when the *n* represents all positive integers.

$$(4n-1)\frac{f_s}{2} \geq f \geq (4n-3)\frac{f_s}{2} \tag{2.2.5}$$

Since $f_s/2$ is Nyquist frequency, from Equation 2.2.5, the high order image components of 1-bit BP-DS modulated signal at specific $(4n-1)^{th}$ and $(4n-2)^{th}$ Nyquist zone can be enhanced by using Manchester coding, as shown in Figure 2.6.

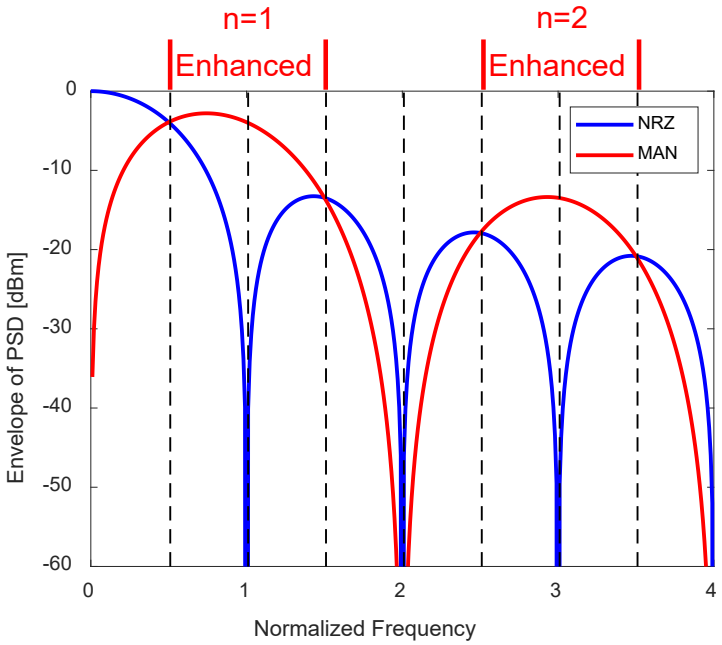

Figure 2.6: Comparison between the calculation results of PSD of NRZ and Manchester code

In this thesis, to ensure the ‘distance‘ between each image components on spectrum, the center frequency of DS modulator is set to $0.25f_s$, quarter of sampling frequency. Therefore, the image components are generated at $(0.5n+0.25)f_s$, n represents the order of image components. Put f=$(0.5n+0.25)f_s$ into the Equation 2.2.2, 2.2.3, 2.2.4. The output power of fundamental and image components of 1-bit BP-DS modulated signal in NRZ and Manchester code can be calculated. The calculated result of output power is shown in Figure 2.7.

As a result, the high order image components of 1-bit BP-DS modulated signal in Manchester code at specific $(4n-1)^{th}$ and $(4n-2)^{th}$ Nyquist zone can be enhanced by 7.65 dB theoretically compared with that in NRZ code, as shown in Figure 2.7. This is consistent with our intuition that the signals near the odd multiple numbers of sampling frequency are enhanced while signals away from the odd multiple numbers of sampling frequency are suppressed which is mentioned above.

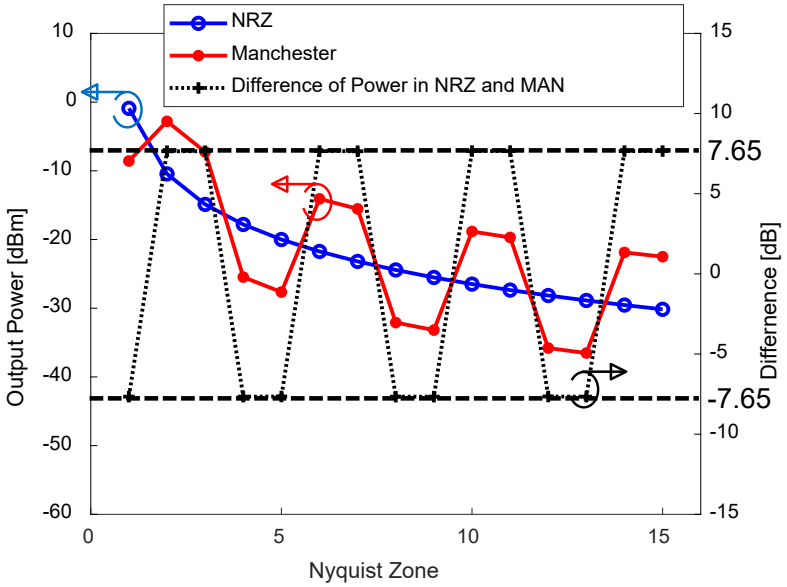

Figure 2.7: Comparison between the calculation results of output power of 1-bit data NRZ and Manchester code

In this section, it is proven by theoretical calculation that the Manchester coding is effective for image enhancement technique in digital domain.

2.3 Evaluation of Image Enhancement Using Manchester Coding

After theoretical calculation, both simulation and measurement are conducted to demonstrate the proposed image enhancement technique using Manchester coding in digital domain in this section.

2.3.1 Simulation result

First, the simulation setup of MATLAB is shown in Figure 2.8. To be consistent with theoretical calculation in previous section, 4^{th} order 1-bit BP-DS modulator in a sampling rate of 8 Gbps is used, and the CW input signal is set at 2.01 GHz near 1/4 f_s. The amplitude is set to $1V_{pp}$. After 1-bit BP-DS modulated data is generated, the NRZ and Manchester encoder is used. To achieve the frequency characteristics, Fourier transform is conducted to 1-bit BP-DS modulated signal in NRZ and Manchester code.

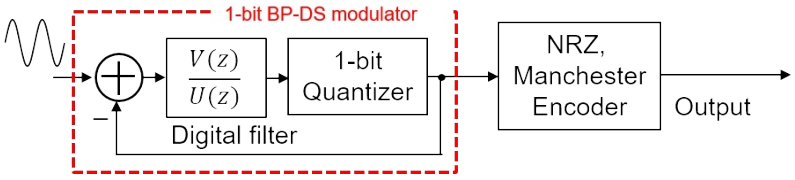

Figure 2.8: Simulation setup

The simulation results of spectrums of 1-bit BP-DS modulated signal in NRZ and Manchester code are presented in Figure 2.9(a), (b), respectively. The simulated output powers of fundamental and image components of 1-bit BP-DS modulated signal in NRZ and Manchester code are picked up and plotted in Figure 2.10. The difference between the simulated output powers of 1-bit BP-DS modulated signal in NRZ and Manchester code in calculation and simulation is concluded in Table 2.1.

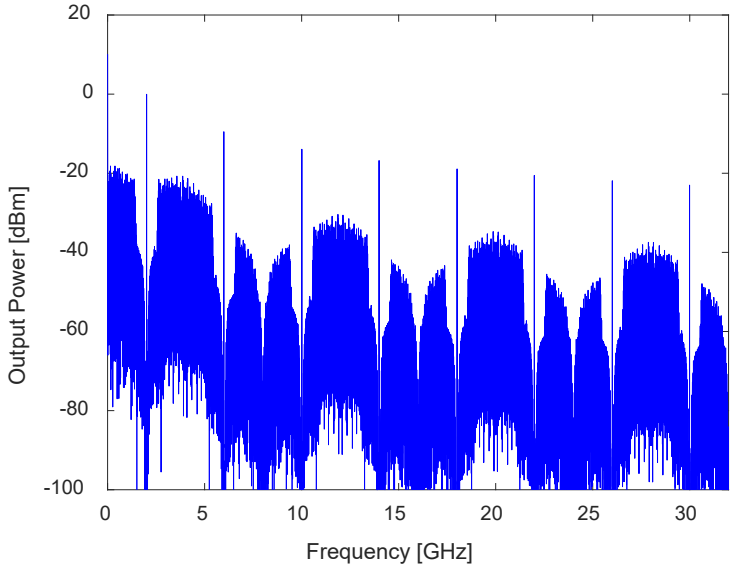

(a) 1-bit BP-DS modulated signal in NRZ code

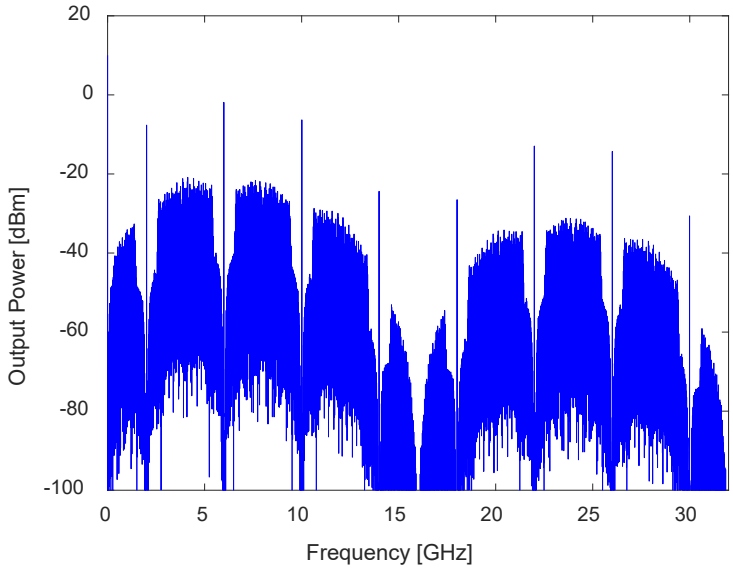

(b) 1-bit BP-DS modulated signal in Manchester code

Figure 2.9: Simulation results of spectrums

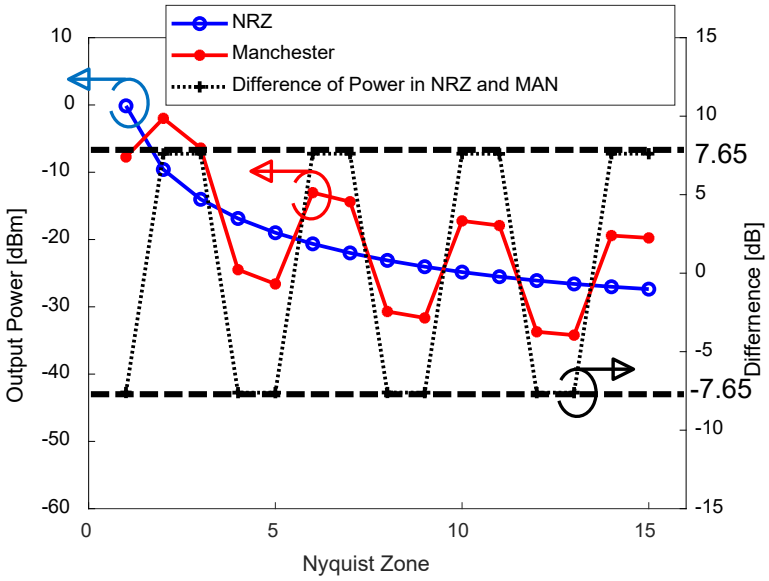

Figure 2.10: Simulated Output powers of fundamental and image components of 1-bit BP-DS modulated signal in NRZ and Manchester code

From Figure 2.10, it can be confirmed that the high order image components of 1-bit BP-DS modulated signal in Manchester code at specific $(4n-1)^{th}$ and $(4n-2)^{th}$ Nyquist zone can be enhanced.

From Table 2.1, it can be confirmed that the enhancement by using Manchester code is very close to theoretical calculation, which proves our proposed image enhancement technique using Manchester code in digital domain effective and feasible.

Table 2.1: Difference value of simulated output power between NRZ and Manchester code.

Nyquist Zone	Difference value [dB]	
	Calculation	Simulation
1	-7.65	-7.60
2	7.65	7.60
3	7.65	7.61
4	-7.65	-7.61
5	-7.65	-7.61
6	7.65	7.61
7	7.65	7.61

2.3.2 Measurement result

To make a further confirmation of proposed image enhancement technique using Manchester code in digital domain, the measurement is conducted as following. The measurement setup is very simple, as shown in in Figure 2.11. After 1-bit digital data is generated by 1-bit BP-DS modulator in MATLAB. The data is inputted into the PPG to generate 1-bit signal. The sampling rate and amplitude are 8 Gps and $1V_{pp}$, same as simulation. The spectrums of 1-bit BP-DS modulated signal in NRZ, and Manchester code are measured by spectrum analyzer with the RBW of 100 KHz.

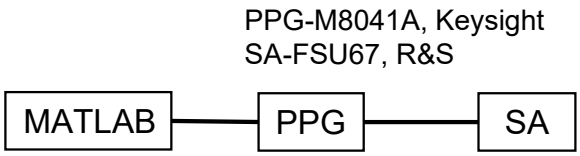

Figure 2.11: Measurement setup

The measured spectrums of 1-bit BP-DS modulator in NRZ and Manchester code are shown in Figure 2.12 (a), (b), respectively. As well as the simulation results, the envelope of measured spectrums of 1-bit BP-DS modulator in NRZ and Manchester code has a good agreement with the calculation result of PSD which is shown in the Figure 2.6. As a result, in the measurement, it can be confirmed that the high order image components of 1-bit BP-DS modulated signal in Manchester code at specific $(4n-1)^{th}$ and $(4n-2)^{th}$ Nyquist zone can be enhanced as well as in the simulation, which is a further proof of the proposed image enhancement technique using Manchester code in digital domain.

As well as in the simulation, the measured output powers of fundamental and image components of 1-bit BP-DS modulated signal in NRZ and Manchester code are picked up and plotted in Figure 2.13. The difference between the measured output powers of 1-bit BP-DS modulated signal in NRZ and Manchester code in calculation and simulation is concluded in Table 2.2.

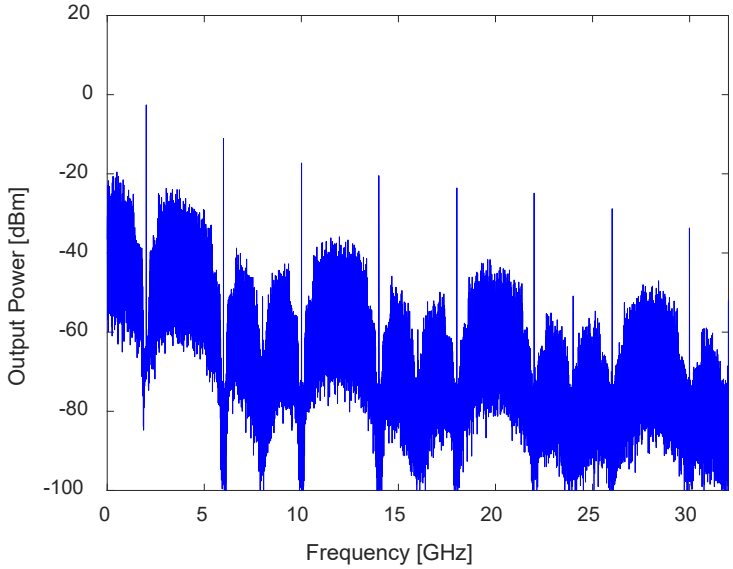

(a) 1-bit BP-DS modulated signal in NRZ code

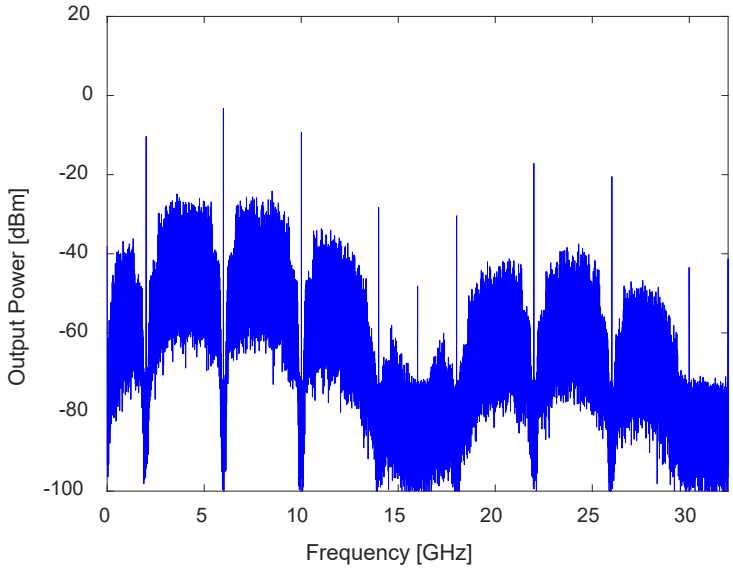

(b) 1-bit BP-DS modulated signal in Manchester code

Figure 2.12: Measurement results of spectrums

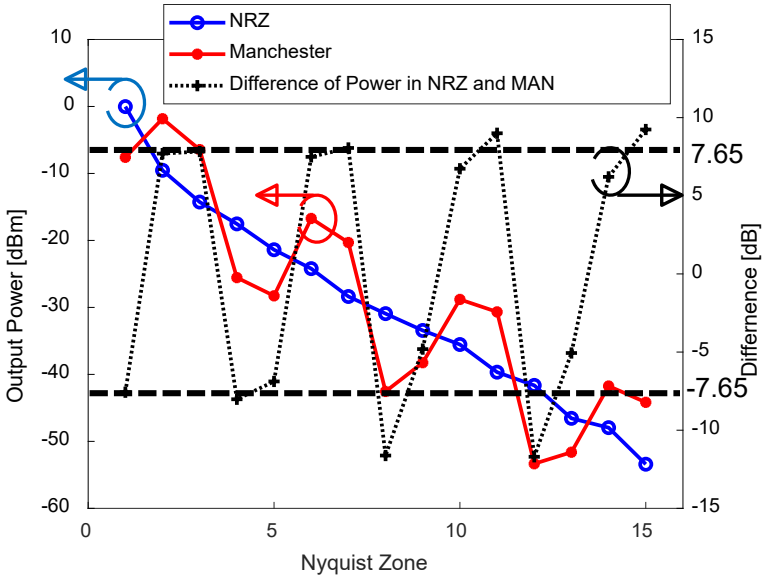

Figure 2.13: Measured Output powers of fundamental and image components of 1-bit BP-DS modulated signal in NRZ and Manchester code

From Table 2.2, it can be confirmed that the enhancement by using Manchester code is very close to theoretical calculation in low frequency, but, with the increasement of frequency, the enhancement deviates from the results of theoretical calculation. The reason for this phenomenon is the frequency response of PPG. In simulation, the ideal 1-bit DAC (encoder) is used to generate ideal 1-bit signal with ideal rising/falling time. However, in measurement, the 1-bit data is generated by PPG with blunt and unbalanced rising/falling edge. As a result, the duty of 1-bit signal is nonideal and the clock leakage can be confirmed in the Figure 2.12.

Table 2.2: Difference value of measured output power between NRZ and Manchester code.

Nyquist Zone	Difference value [dB]	
	Calculation	Measurement
1	-7.65	-7.57
2	7.65	7.70
3	7.65	7.83
4	-7.65	-8.02
5	-7.65	-6.88
6	7.65	7.49
7	7.65	8.06

2.4 Summary

All calculated, simulated and measured output powers of fundamental and image components of 1-bit BP-DS modulated signal in NRZ and Manchester code are concluded in Table 2.3. From Table 2.3, it is confirmed by theoretical calculation, simulation and measurement that the high order image components of 1-bit BP-DS modulated signal in Manchester code at specific $(4n-1)^{th}$ and $(4n-2)^{th}$ Nyquist zone can be enhanced. As mentioned above, the simulation result has a good agreement to the calculation result even though the measurement result deviates slightly from the calculation result in high frequency band because of the frequency response of measurement device, PPG. Therefore, it is proven that the proposed image enhancement technique using Manchester coding in digital domain is effective and feasible. In addition, since our proposal is using Manchester coding in digital domain and the Manchester coding can be easily implemented by XOR gate, the deviation in the measurement is not so critical.

Table 2.3: Conclusion of output powers of 1-bit BP-DS modulated signal in NRZ and Manchester code.

Nyquist Zone	Calculation			Simulation			Measurement		
	NRZ [dBm]	MAN [dBm]	Diff. [dB]	NRZ [dBm]	MAN [dBm]	Diff. [dB]	NRZ [dBm]	MAN [dBm]	Diff. [dB]
1	-0.91	-8.56	-7.65	-0.13	-7.73	-7.60	-0.02	-7.59	-7.57
2	-10.45	-2.8	7.65	-9.59	-1.99	7.60	-9.53	-1.83	7.70
3	-14.89	-7.24	7.65	-14.02	-6.41	7.61	-14.27	-6.44	7.83
4	-17.81	-25.46	-7.65	-16.84	-24.48	-7.61	-17.53	-25.55	-8.02
5	-20.00	-27.65	-7.65	-18.99	-26.60	-7.61	-21.39	-28.27	-6.88
6	-21.74	-14.09	7.65	-20.64	-13.03	7.61	-24.21	-16.72	7.49
7	-23.19	-15.54	7.65	-21.99	-14.38	7.61	-28.37	-20.31	8.06

Chapter 3

Image Enhancement Technique Using RF Tripler in Analog Domain

In previous chapter, an image enhancement technique using Manchester coding in digital domain has been proposed and illustrated. However, as mentioned above, the attenuation of high order image components is caused not only by NRZ coding scheme in digital domain but also by the frequency characteristics of 1-bit DAC in analog domain. Even though the high order image components of 1-bit BP-DS modulated signal are enhanced by 7.6 dB, a severe attenuation beyond ten to dozens of decibels still will occur in analog domain. Consequently, an image enhancement technique in analog domain is necessary as well. In this chapter, to enhance or regenerate the high order image components of 1-bit BP-DS modulated signal, an image enhancement technique using RF tripler in analog domain is proposed to be implemented after 1-bit DAC. Compared to the conventional transmitter using up-converter, it obvious that transmitter using RF tripler has a simpler architecture, which is easier to implement in practical, so that the miniaturization of transmitter can be achieved as well even in direct digital RF transmitter using the high order (5^{th} or 6^{th}) image components of 1-bit BP-DS modulated signal. It is proven by theoretical calculation, simulation and measurement that the high order image components of 1-bit BP-DS modulated signal in Manchester code can be regenerated by RF tripler with a good performance of noise shaping.

3.1 Principle of image enhancement technique using RF tripler

In [41], it has been proven that 1-bit DAC based on inverter can enhance or regenerate the high order image components of lowpass filtered 1-bit BP-DS modulated signal by sharpening the rising/falling time of signal.

However, it is just phenomenon-based observation and can not explain the principle. To illustrate the principle of image enhancement, the behaviour of 1-bit DAC based on inverter should be modelized mathematically and specifically. Since it is a nonlinear device, its output-input function in time domain can be simplified by (3.1.1).

$$y(t) = \sum_{i=0}^{+\infty} a_i * x^i(t) \tag{3.1.1}$$

Obviously, the image components can only be regenerated or enhanced by its nonlinear response. So the theoretical calculation of its nonlinear response when n is supposed to be 2 (doubler) and 3 (tripler) will be conducted in this section to explain the principle of image enhancement.

As RF multiplier, a nonlinear device, the ideal output-input function in time domain can be simplified by (3.1.2) [42–44].

$$y(t) = a * x^n(t). \tag{3.1.2}$$

n is order of RF multiplier, supposed to be 2 and 3, in the calculation of RF douber and tripler, respectively. Consequently, the input signal can only be consisted of the fundamental and low order image components since the high order image components of 1-bit BP-DS modulated signal, whose frequency is higher than bitrate, attenuate severely because of the frequency characteristics of 1-bit DAC.

As image enhancement technique using Manchester coding has been proposed in the previous section, 1-bit BP-DS modulated signal in Manchester coding is used in calculation. Since the Manchester coding was proposed to enhance the image components at specific $(4n\text{-}1)^{th}$ and $(4n\text{-}2)^{th}$ Nyquist Zone, only the 1^{st} and 2^{nd} image components of 1-bit BP-DS

modulated signal are regarded as input signal after suffering a severe attenuation from 1-bit DAC. As a result, to simplify the calculation, it is supposed that a is normalized and input signal x(t)=Acos($2\pi f_{RF}$t)+Bcos[$2\pi(2f_s - f_{RF})$t] in CW condition while $f_{RF} = 0.75f_s$ is the frequency of RF signal and f_s is datarate which is half of the bitrate. After the calculation, the output signals y(t) of RF doubler and tripler are shown in (3.1.3) and (3.1.4), respectively.

3.1.1 Using RF doubler in the enhancement technique

$$\begin{aligned} y_{doubler}(t) &= \{Acos(2\pi f_{RF}t) + Bcos[2\pi(2f_s - f_{RF})t]\}^2 \\ &= 0.5A^2cos(2\pi * 2f_{RF}t) + 0.5B^2cos[2\pi(4f_s - 2f_{RF})t] \\ &\quad + ABcos(2\pi * 2f_st) + ABcos[2\pi(2f_s - 2f_{RF})t] \\ &\quad + 0.5(A^2 + B^2) \end{aligned} \tag{3.1.3}$$

Obviously, from (3.1.3), there is no fundamental or image components in the output signal of RF doubler. So, theoretically, the RF doubler can not be used to enhance or regenerate the high order image component.

3.1.2 Using RF tripler in the enhancement technique

$$\begin{aligned} y_{tripler}(t) &= \{Acos(2\pi f_{RF}t) + Bcos[2\pi(2f_s - f_{RF})t]\}^3 \\ &= \underline{(0.75A^3 + 1.5AB^2)cos(2\pi f_{RF}t)} \\ &\quad \underline{+(0.75B^3 + 1.5A^2B)cos[2\pi(2f_s - f_{RF})t]} \\ &\quad \underline{+0.75A^2Bcos[2\pi(2f_s + f_{RF})t]} \\ &\quad \underline{+0.75AB^2cos[2\pi(4f_s - f_{RF})t]} \\ &\quad \underline{+0.25A^3cos(2\pi * 3f_{RF}t)} \\ &\quad \underline{+0.75A^2Bcos[2\pi(2f_s - 3f_{RF})t]} \\ &\quad \underline{+0.75AB^2cos[2\pi(4f_s - 3f_{RF})t]} \\ &\quad \underline{+0.25B^3cos[2\pi(6f_s - 3f_{RF})t]} \end{aligned} \tag{3.1.4}$$

However, from (3.1.4), in the output signal of tripler, there are fundamental and image components (f_{RF}) which are marked by solid line and third harmonic components ($3f_{RF}$)which are marked by dash line. Obviously, the third harmonic components are undesired interference signal. For the modulation signal, the bandwidth of third harmonic components is three times wider than the fundamental and image components. Nevertheless, it still can be confirmed that the high order image components whose frequency is beyond the bitrate are regenerated by RF tripler.

The theoretical calculation can be extended to higher order RF multiplier, such as RF quadrupler, quintupler and so on. As a result, the high order image component of lowpass filtered 1-bit BP-DS modulated signal can only be regenerated by odd-order RF multiplier instead of even-order RF multiplier.

3.2 Theoretical calculation by using 1-bit BP-DS modulated signal in both NRZ and Manchester code

Previously, the principle of image enhancement using RF tripler has been illustrated qualitatively. However, to verify it by the simulation and measurement, quantitative calculation is necessary. The calculation result using RF tripler under the condition of NRZ and Manchester code is shown as follows. Different from Manchester signal, the fundamental and 1^{st} componens of 1-bit BP-DS modulated signal in NRZ code is regarded as input signal because of the attenuation in Sinc function. Consequently, in the condition of NRZ code, the input signal is supposed to be x(t)=Acos($2\pi f_{RF}$t)+Bcos[$2\pi(f_s - f_{RF})$t] while $f_{RF} = 0.25f_s$ is the frequency of RF signal and f_s is datarate which is equal to the bitrate.

The input signals of RF tripler in the condition of 1-bit BP-DS modulated signal in NRZ and Manchester code are shown in Figure 3.1(a), (b), respectively. The amplitude of input signals can be calculated by Equation 2.2.2 and 2.2.3 in previous section. After calculation by y(t) = $x^3(t)$, the amplitude of output signals of RF tripler in the condition of 1-bit BP-DS modulated signal in NRZ and Manchester code are shown in Figure 3.2(a), (b), respectively. The harmonic and regenerated image components are shown in red and blue, respectively.

In NRZ code condition, since the frequency of input signal is lower than that in Manchester code, only 2^{nd} and 3^{rd} order image components are regenerated. The regenerated image components are overlapped by harmonic components, which will degrade SNR. As introduced in chapter 1, because the upper limit of sampling frequency of DSP is about 6GHz, to generate RF signal at 20 GHz-band or above, it is necessary to utilize the high order image components beyond 5^{th} order. In contrast, with higher frequency of input signal in Manchester code, it is confirmed that 5^{th} and 6^{th} order image components of 1-bit BP-DS modulated signal are regenerated, which meet the requirements described above. Moreover, in Manchester code condition, the harmonic components are totally separated from the regenerated image components, which improves the SNR. As a result, it is proven that using RF tripler can regenerated the high order image components and a better performance can be achieved by using Manchester coding additionally, compared with NRZ coding.

In this section, the principle of image enhancement technique using RF tripler in analog domain is illustrated first. With an ideal mathematical model of RF multiplier, it is confirmed that the high order image components of 1-bit BP-DS modulated signal can only be regenerated by RF tripler or odd-order RF multiplier. With a detailed quantitative calculation, the regenerated high order image components of 1-bit BP-DS modulated signal in Manchester by using RF tripler has a better performance in higher frequency, compared with that in NRZ code.

In addition, it must be noticed that the calculation is conducted using an ideal model, $y(t)=x^3(t)$. Obviously, it has not taken the practical implementation into the consideration which leads the limitation in practical. As shown in (3.1.4), the output power of RF tripler will degrade/increase by 3 dB as the input power degrades/increases by 1 dB. But, actually, in the practical implementation, as nonlinear RF device, the RF tripler is usually implemented by transistors or diodes which are biased around the saturation or pinch-off region. It limits the conversion gain. As a result, the output power is limited in practical implementation because of the device characteristics. However, even if there are some limitations of the ideal calculation, the result of theoretical calculation can explain the principle of the

proposed image enhancement technique using RF tripler qualitatively and has a good agreement to simulation and measurement in CW condition which will be shown in the following sections.

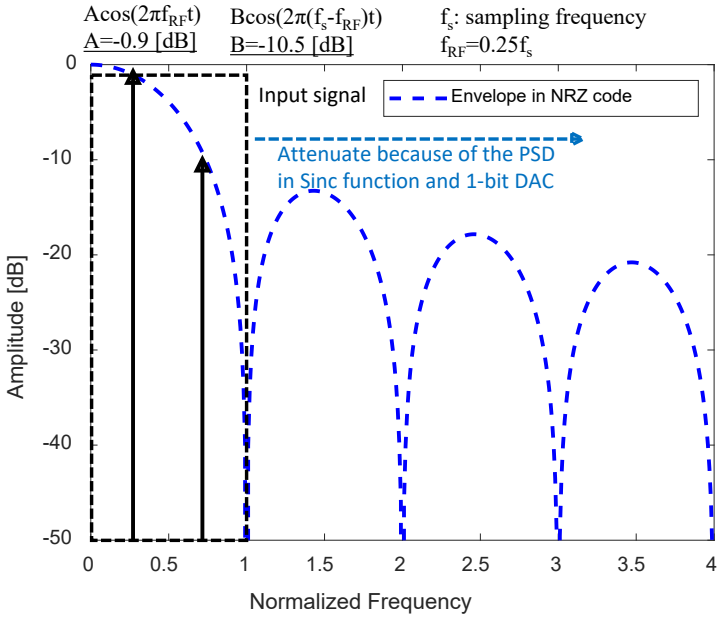

(a) NRZ code

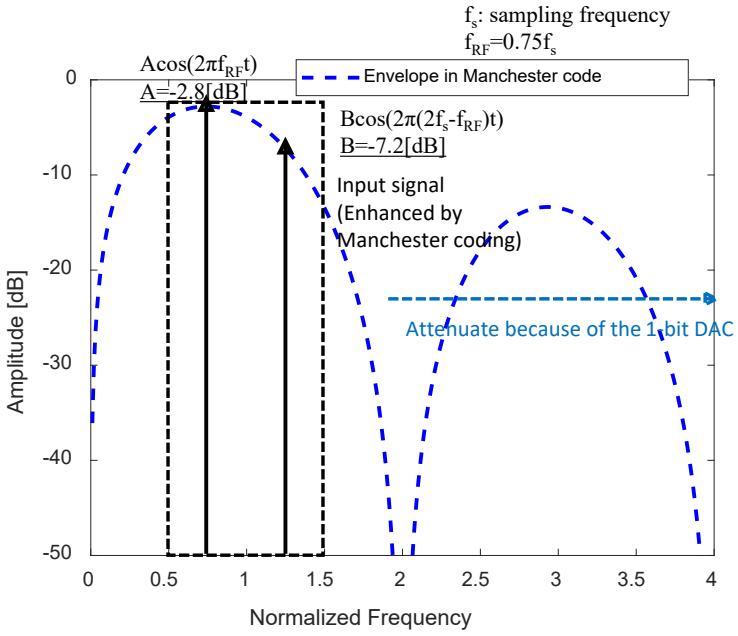

(b) Manchester code

Figure 3.1: Input signals of RF tripler

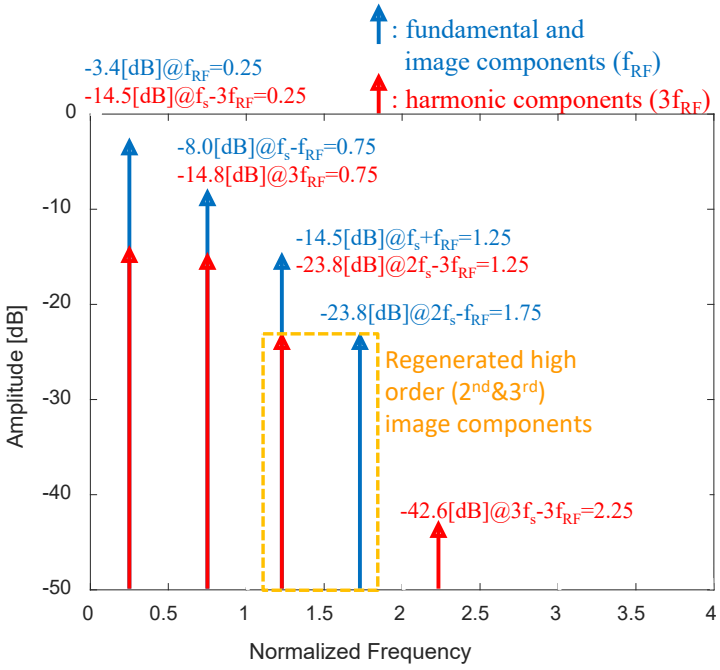

(a) NRZ code

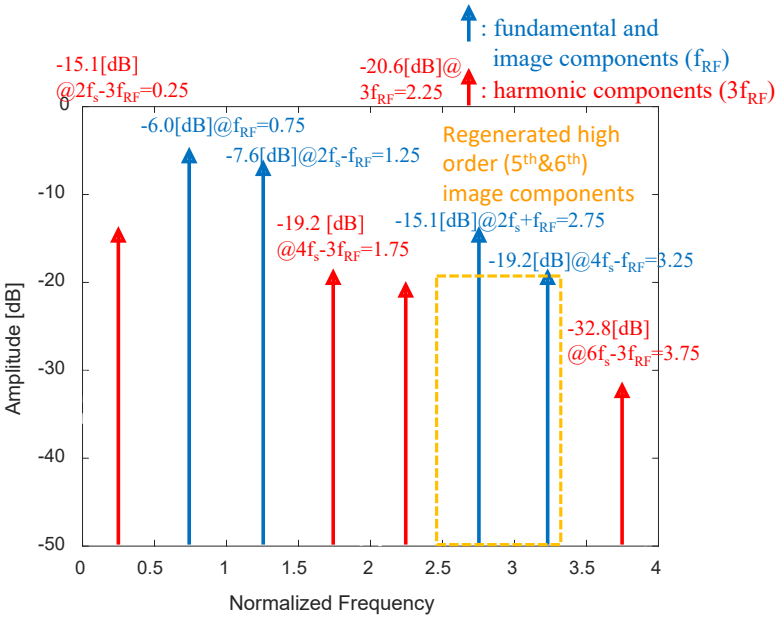

(b) Manchester code

Figure 3.2: Output signals of RF tripler

3.3 Evaluation of image enhancement technique using RF tripler

After theoretical calculation, for further demonstration of the proposed image enhancement technique using RF tripler, both simulation and measurement are conducted in this section.

3.3.1 Simulation result

First, the RF signal whose frequency is 0.501 GHz is modulated to ideal 1-bit digital signal in NRZ and Manchester code whose amplitude and datarate are $1V_{pp}$ and 2 Gbps, respectively. The ideal Butterworth lowpass filter whose cutoff frequency is 3.5 GHz is applied to imitate the frequency characteristics of 1-bit DAC, which is consistent with measurement setup. The lowpass filtered 1-bit BP-DS modulated signals in both NRZ and Manchester code are regarded as input signal of ideal RF tripler. The simulation setup is shown in Figure 3.3.

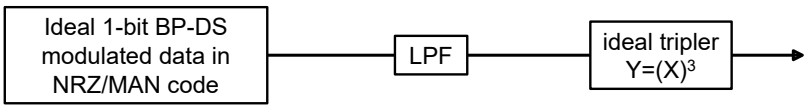

Figure 3.3: Simulation setup

By comparing the spectrums of input and output signals of ideal RF tripler, it is able to confirm if the high order image components can be regenerated.

The waveform and spectrum of ideal 1-bit BP-DS modulated signal in NRZ code is shown in Figure 3.4(a), (b), respectively. The waveform and spectrum of ideal 1-bit BP-DS modulated signal in Manchester code is shown in Figure 3.5(a), (b), respectively. With the ideal rising/ falling edge, the high order image components can be generated and observed with a good performance of noise shaping.

The simulated spectrums of input and output signals of ideal RF tripler using 1-bit BP-DS modulated signal in NRZ and Manchester code are shown in Figure 3.6 and 3.7, respectively.

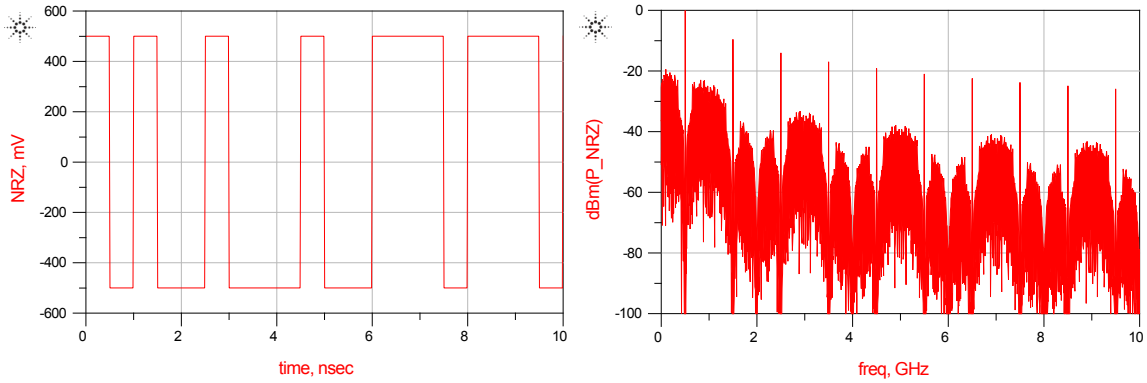

(a) Waveform (b) Spectrum

Figure 3.4: Simulation result of ideal 1-bit BP-DS modulated signal in NRZ code

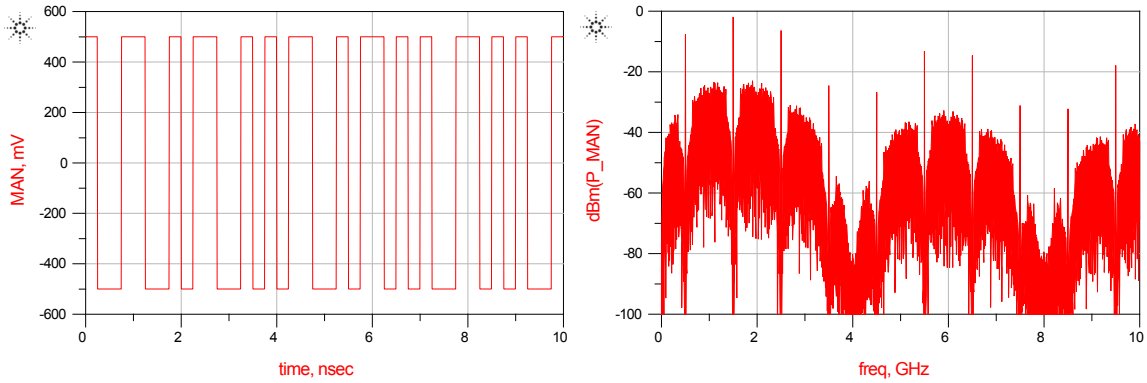

(a) Waveform (b) Spectrum

Figure 3.5: Simulation result of ideal 1-bit BP-DS modulated signal in Manchester code

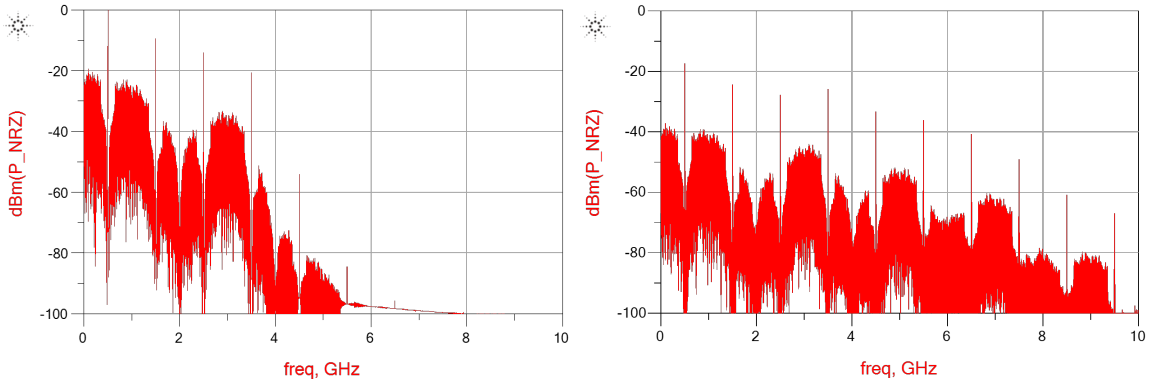

(a) Input spectrum of ideal RF tripler (b) Output spectrum of ideal RF tripler

Figure 3.6: Simulation result of image enhancement technique using RF tripler in NRZ code condition

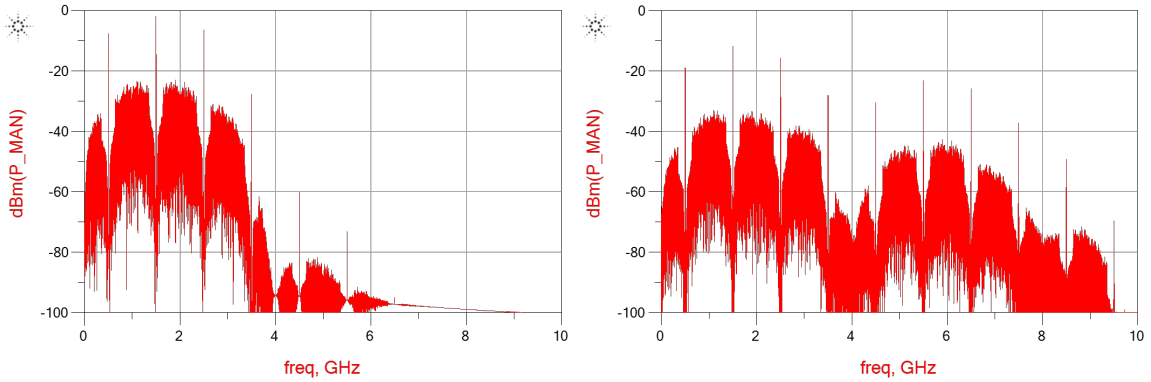

(a) Input spectrum of ideal RF tripler (b) Output spectrum of ideal RF tripler

Figure 3.7: Simulation result of image enhancement technique using RF tripler in Manchester code condition

Obviously, the high order image components of 1-bit BP-DS modulated signal in both NRZ and Manchester code are regenerated or enhanced by RF tripler because of its non-linearity. Meanwhile, the output power of regenerated high order image components in Manchester code condition is much higher than that in NRZ code condition. To confirm the noise shaping characteristics and output power of the regenerated high order image components, the enlarged spectrums at 5.5 GHz and 6.5 GHz of 5^{th} and 6^{th} order image components in NRZ and Manchester code condition are shown in Figure 3.8 and 3.9, respectively.

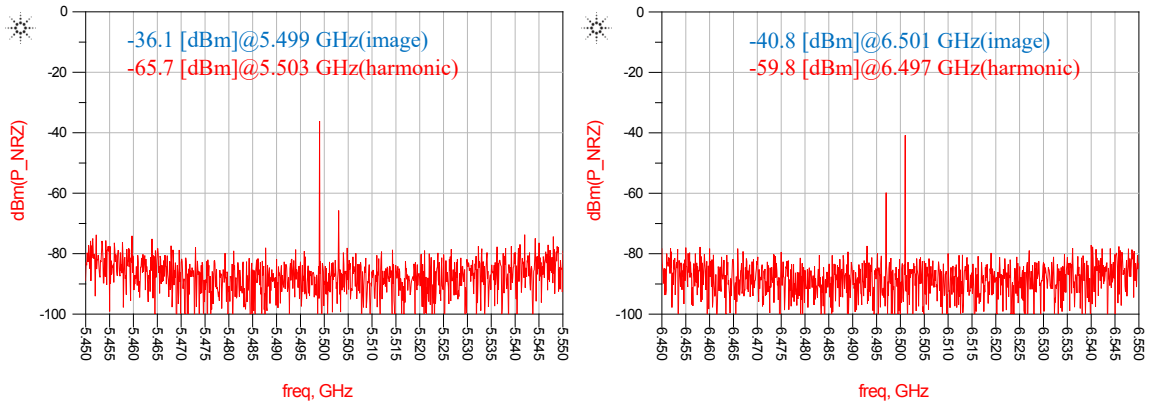

(a) Enlarged spectrum at 5.5 GHz

(b) Enlarged spectrum at 6.5 GHz

Figure 3.8: Enlarged spectrums of output signal of RF tripler in NRZ code condition in simulation

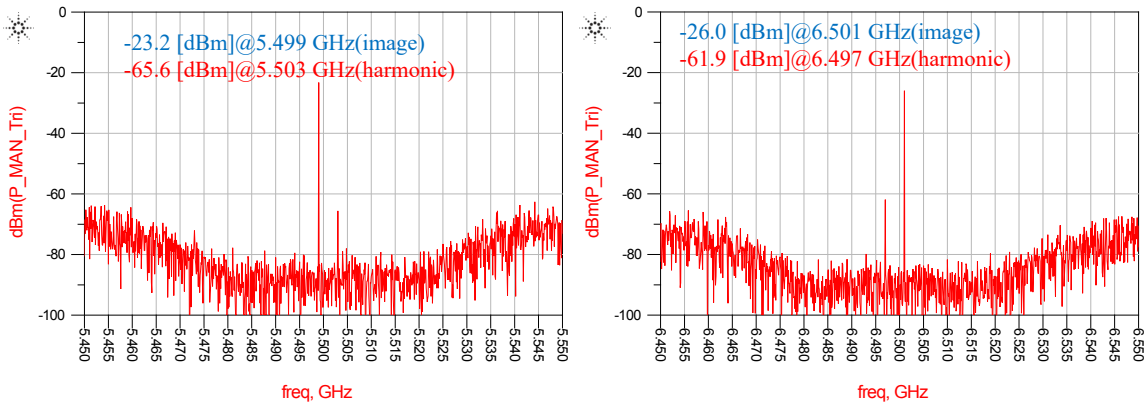

(a) Enlarged spectrum at 5.5 GHz

(b) Enlarged spectrum at 6.5 GHz

Figure 3.9: Enlarged spectrums of output signal of RF tripler in Manchester code condition in simulation

From Figure 3.8 and 3.9, the high order image components of 1-bit BP-DS modulated signal in Manchester code are regenerated in beyond 10dB higher output power with a better noise shaping characteristics than that in NRZ code. Since the simulation results show a good agreement with the calculation result, it is proven that RF tripler can regenerate the high order image components of 1-bit BP-DS modulated signal, which suffer a severe attenuation because of the frequency characteristics of 1-bit DAC, and using Manchester coding, which is proposed to enhance the image components in digital domain in previous section, before RF tripler can improve the output power and noise shaping characteristics of regenerated high order image components.

In addition, in the theoretical calculation, since only 1^{st} and 2^{nd} image components of 1-bit BP-DS modulated signal in Manchester code is regarded as input signal, the harmonic components, as unused signal, are separated. But, in the simulation, the fundamental component is also part of input signal of RF tripler, so there are still some harmonic components close to image components that can be confirmed. Meanwhile, it's important that the power of harmonic components is about 35 dB lower than that of regenerated image components, which can prove our assumption and calculation reasonable in certain degree.

It is predictable that in the condition of modulation wave, the adjacent channel leakage ratio (ACLR) can be beyond 40 dB theoretically. The simulated output power of regenerated image components in Manchester code condition is about 7 dB lower than the calculated one. Maybe it is because the noise components have not been considered in calculation. In the future work, noise components shall be modelized as well.

3.3.2 Measurement result

The measurement setup is shown in Figure 3.10. Instead of ideal LPF and Tripler using in simulation, the practical LPF (VLFG3500+, Mini-circuit) whose cutoff frequency is 3.5 GHz and Tripler (ZX90-3-692-S +, Mini-circuit) whose input frequency is from 1.7 GHz to 2.3 GHz are used in measurement. Meanwhile, in measurement, waveforms are observed by oscilloscope (M8020A, Keysight) and spectrums are obtained by FFT using MATLAB. CW signal whose frequency is 0.501 GHz is used as original RF signal in measurement, same as in simulation. The parameter of 1-bit BP-DS modulated data is same as simulation as well, but generated by PPG (M18020A, Anritsu). The measurement results are presented as following.

Figure 3.10: Measurement setup

The waveforms and spectrums of 1-bit BP-DS modulated signal in NRZ and Manchester code are shown in Figure 3.11 and 3.12, respectively. Different from ideal 1-bit signal in simulation, 1-bit signal is generated by PPG in measurement. Therefore, the rising/falling edge is not ideal so that the high order image components of 1-bit BP-DS modulated signal shall attenuate. However, since the maximum bitrate of PPG is 32 Gbps, much higher than datarate, 2Gbps, the 5^{th} and 6^{th} order image components at 5.5 GHz and 6.5 GHz can be still observed with high output power level.

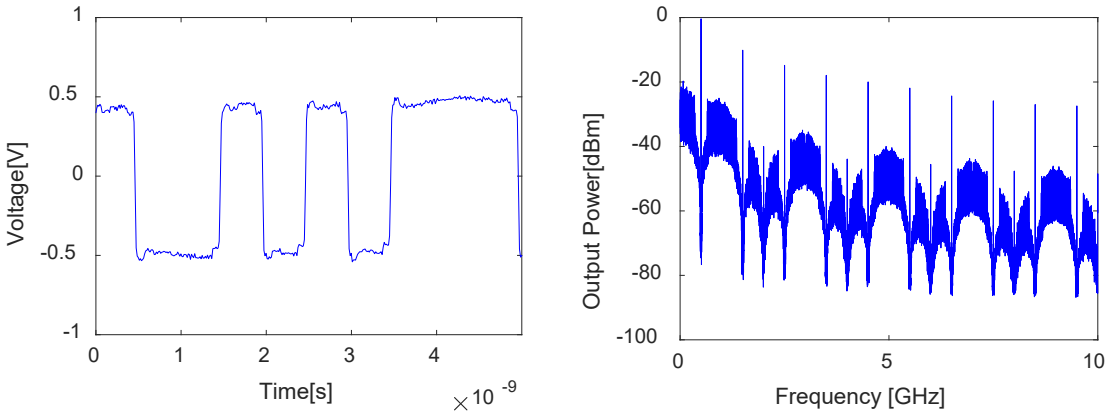

(a) Waveform (b) Spectrum

Figure 3.11: Measurement result of 1-bit BP-DS modulated signal in NRZ code

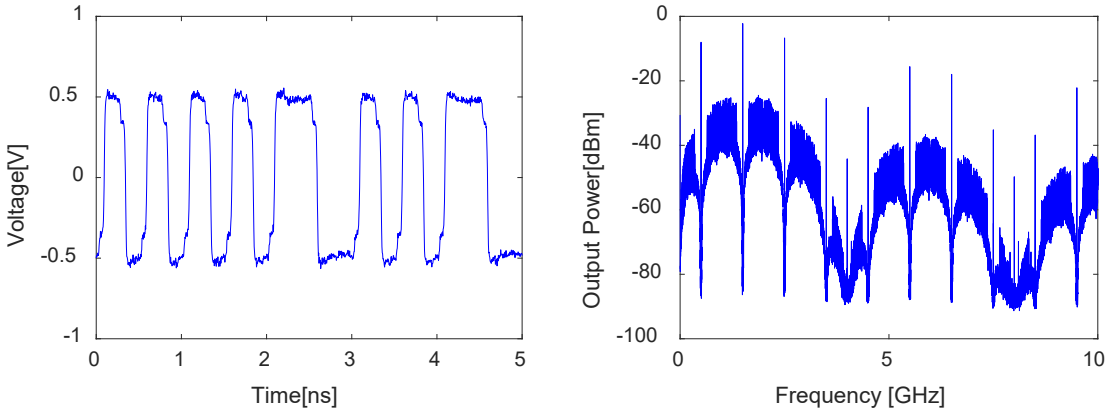

(a) Waveform (b) Spectrum

Figure 3.12: Measurement result of 1-bit BP-DS modulated signal in Manchester code

As mentioned in chapter1, the maximum sampling frequency of DSP is about 6 Gbps. To imitate the frequency characteristics of 1-bit DAC in DSP, the LPF is inserted between PPG and RF tripler in measurement, same as in simulation. The lowpass-filtered 1-bit signal is regarded as input signal of RF tripler. From the measured output signal of RF tripler, it can be confirmed if the high order image components of 1-bit BP-DS modulated signal can be generated in measurement. The measured spectrums of input and output signals of ideal RF tripler using 1-bit BP-DS modulated signal in NRZ and Manchester code are shown in Figure 3.13 and 3.14, respectively.

As well as in simulation, the attenuated high order image components of 1-bit BP-DS modulated signal in both NRZ and Manchester code can be regenerated by RF tripler in measurement. From the Figure 3.14, the measured output power of regenerated high order image components in Manchester code condition is much higher than that in NRZ code condition. To confirm the noise shaping characteristics and output power of the regenerated high order image components, the enlarged spectrums at 5.5 GHz and 6.5 GHz of 5^{th} and 6^{th} order image components in NRZ and Manchester code condition are shown in Figure 3.15 and 3.16, respectively.

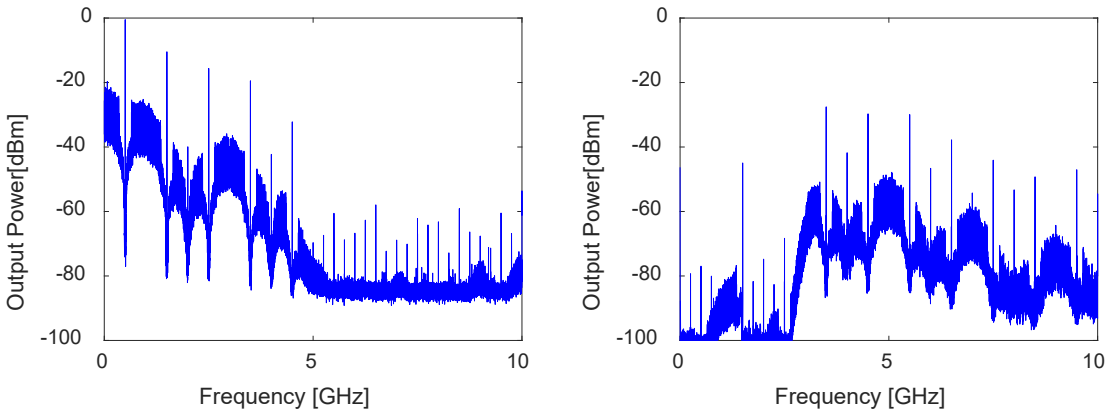

(a) Input spectrum of ideal RF tripler (b) Output spectrum of ideal RF tripler

Figure 3.13: Measurement result of image enhancement technique using RF tripler in NRZ code condition

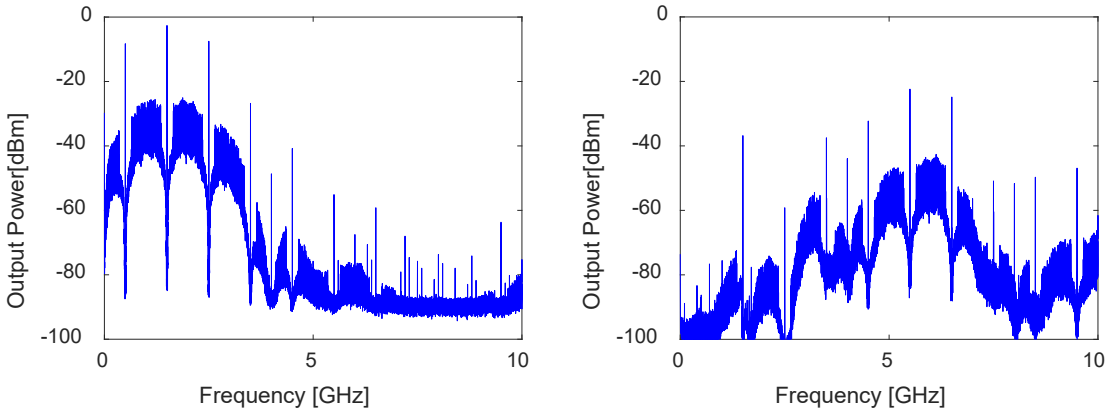

(a) Input spectrum of ideal RF tripler (b) Output spectrum of ideal RF tripler

Figure 3.14: Measurement result of image enhancement technique using RF tripler in Manchester code condition

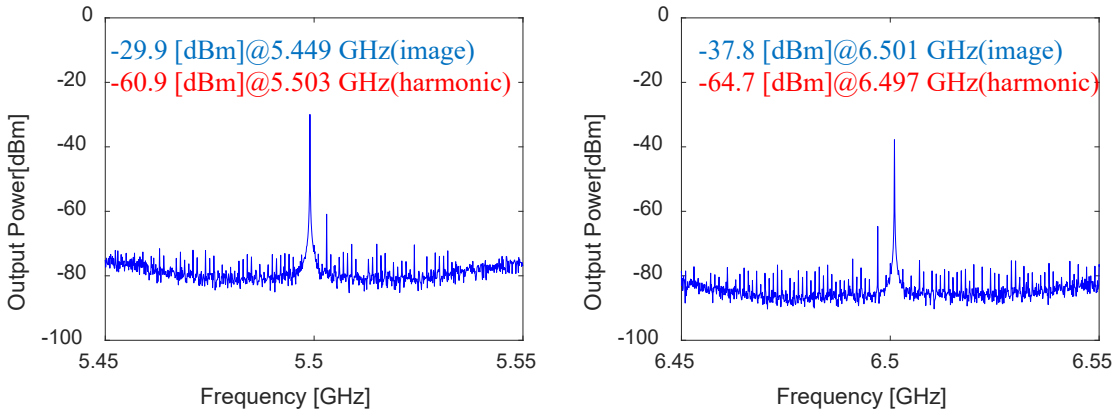

(a) Enlarged spectrum at 5.5 GHz (b) Enlarged spectrum at 6.5 GHz

Figure 3.15: Enlarged spectrums of output signal of RF tripler in NRZ code condition in measurement

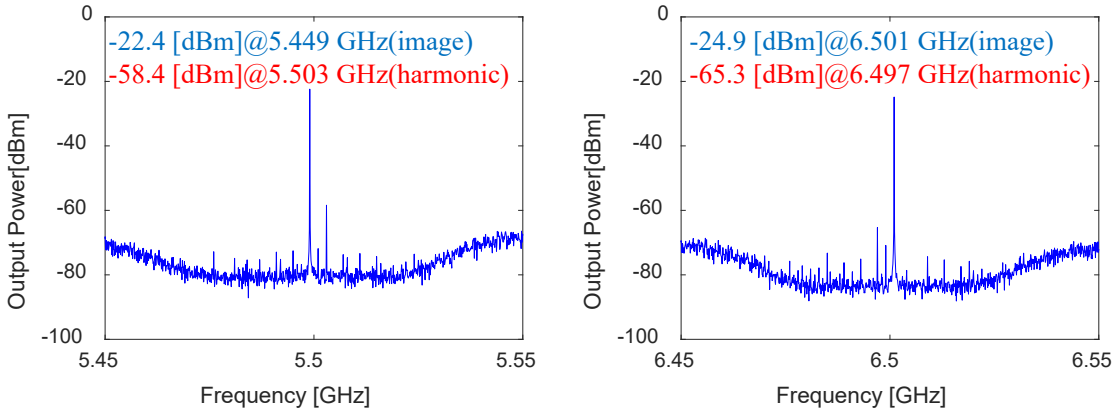

(a) Enlarged spectrum at 5.5 GHz (b) Enlarged spectrum at 6.5 GHz

Figure 3.16: Enlarged spectrums of output signal of RF tripler in Manchester code condition in measurement

From the enlarged spectrums shown in Figure 3.15 and 3.16, the output powers of regenerated high order image components at 5.5 GHz and 6.5 GHz of 1-bit BP-DS modulated signal in Manchester code are -22.4 dBm and -24.9 dBm, which are much higher and has a better performance of noise shaping than that in NRZ code. Since the powers of harmonic components in NRZ and Manchester code condition are very close, consequently, the regenerated high order image components at 5.5 GHz and 6.5 GHz of 1-bit BP-DS modulated signal in Manchester code have a better performance on SNR. The measurement results using 1-bit BP-DS modulated signal in Manchester code have a good agreement with the simulation, which prove the proposed image enhancement technique using RF tripler in analog domain effective and feasible.

3.4 Summary

The simulated and measured output powers of the regenerated high order image components of 1-bit BP-DS modulated signal in NRZ and Manchester code are concluded in Table 3.1. From Table 3.1, it is confirmed by theoretical calculation, simulation and measurement that the high order image components of 1-bit BP-DS modulated signal can be enhanced or regenerated despite suffering a severe attenuation because of the frequency characteristics of 1-bit DAC. Moreover, compared with the NRZ coding scheme, using Manchester coding can improve the output power of regenerated high order image components of 1-bit BP-DS modulated signal beyond 10 dB. Although there is some difference between the simulation and measurement, which may be caused by nonideal measurement device, the simulation and measurement results are still good evidence to prove the proposed image enhancement technique using RF tripler in analog domain effective and feasible and make it convincible that the high order image components can be regenerated by nonlinear device which is the principle of this chapter.

Since the frequency is normalized in the theoretical calculation, the effectiveness of proposed image enhancement technique using Manchester coding and RF tripler is irrelevant to frequency, which means it should be effective in any frequency band as well.

Table 3.1: Conclusion of output powers of 1-bit BP-DS modulated signal in NRZ and Manchester code.

Order of regenerated image component	Simulation			Measurement		
	NRZ [dBm]	MAN [dBm]	Diff. [dB]	NRZ [dBm]	MAN [dBm]	Diff. [dB]
5^{th}@5.5 GHz	-36.1	-23.2	12.9	-29.9	-22.4	7.5
6^{th}@6.5 GHz	-40.8	-26.0	14.2	-37.8	-24.9	12.9

Chapter 4

Low-Backlobe 4-Element Endfire Vivaldi Array Antenna

First and foremost, in this thesis, the FBR is defined as the ration of the maximum gain on mainlobe and backlobe (from 150° to 210°). All antenna gain pattern in this chapter is evaluated at 19.33 GHz.

As introduced in chapter 1, to simplify the implementation of DBF transmitter, a low-backlobe endfire array antenna is necessary. In this chapter, a low-backlobe endfire Vivaldi array antenna with two slits is proposed. With two slits on both left and right edges, the FBR of Vivaldi antenna element is improved to 23.5 dB. 4-element Vivaldi array antenna based on two-slit configuration has a good performance of FBR beyond 20 dB in simulation as well. Although only front radiation pattern is measured because of the limitation of measurement system, the measurement result has a good agreement with the simulation result.

4.1 Conventional Vivaldi antenna

TSA is a configuration of planar endfire antenna that can generate beam horizontal to the substrate and classified by the shape of taper [35]. Vivaldi antenna is one of TSA whose taper is shaped by exponential function. Although the gain of Vivaldi antenna is relatively

low, it has the advantage of beamwidth, bandwidth and sidelobe so that Vivaldi antenna is chosen in this thesis. The design of conventional Vivaldi antenna is shown in Figure 4.1.

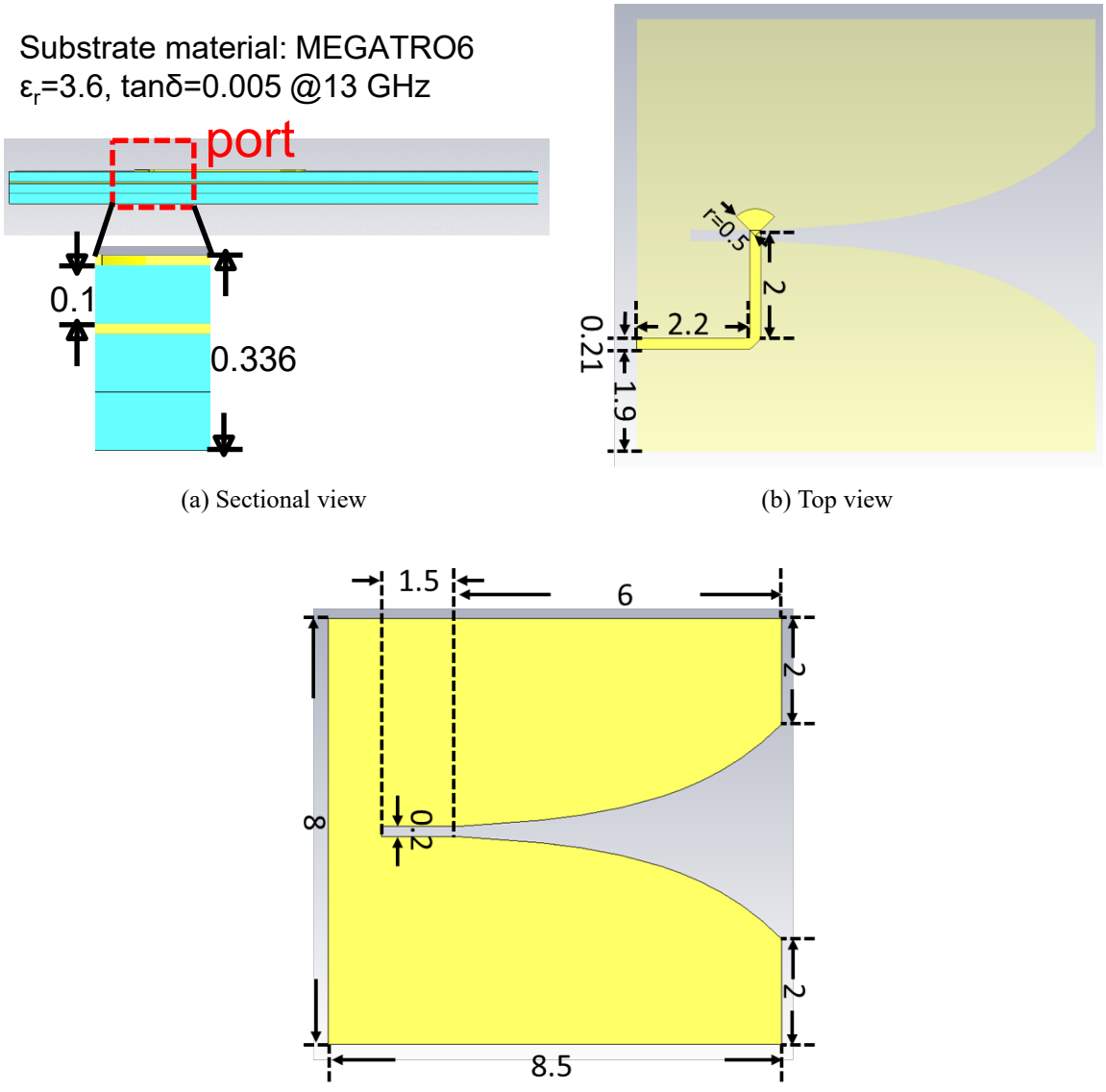

(a) Sectional view

(b) Top view

(c) Bottom view

Figure 4.1: Design of conventional Vivaldi antenna (Unit: mm)

The simulation result of antenna gain pattern is shown in Figure 4.2.

In the simulation, the maximum gain and backlobe level of conventional Vivaldi antenna are 4.9 dBi and -3.6 dBi, respectively, which means the F/B ratio is 8.5 dB and the leaked power from backside of antenna can be reflected to the frontside by DBF transmitter module in practical implementation.

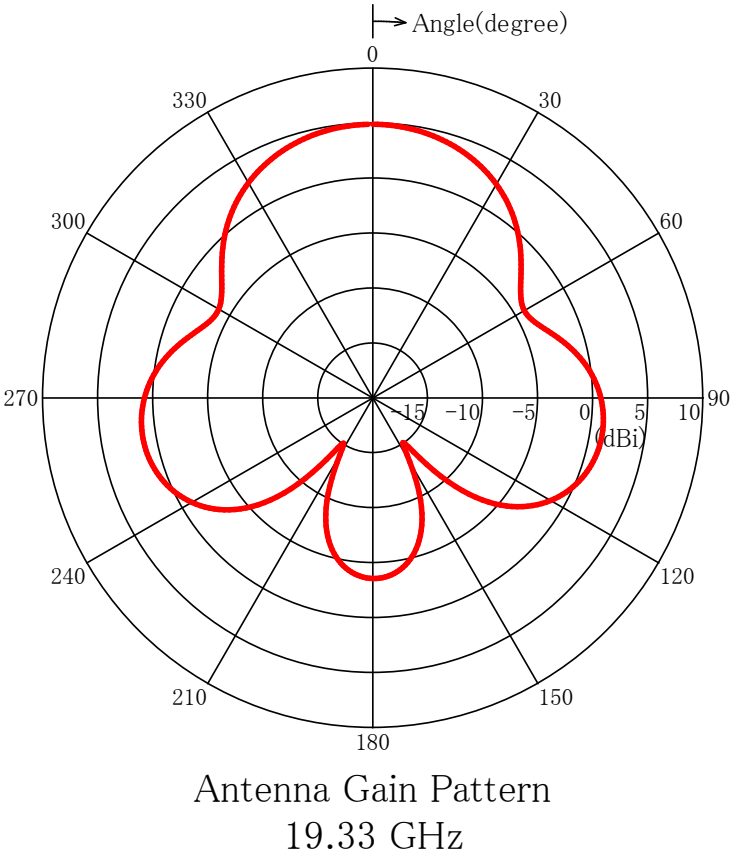

Figure 4.2: Simulated antenna gain pattern of conventional Vivaldi antenna

4.2 Vivaldi antenna with single slit

The mechanism of backlobe has been described in [45]. As shown in Figure 4.3, the backlobe is generated by the current flowing on left and right edge sides. If the current flowing

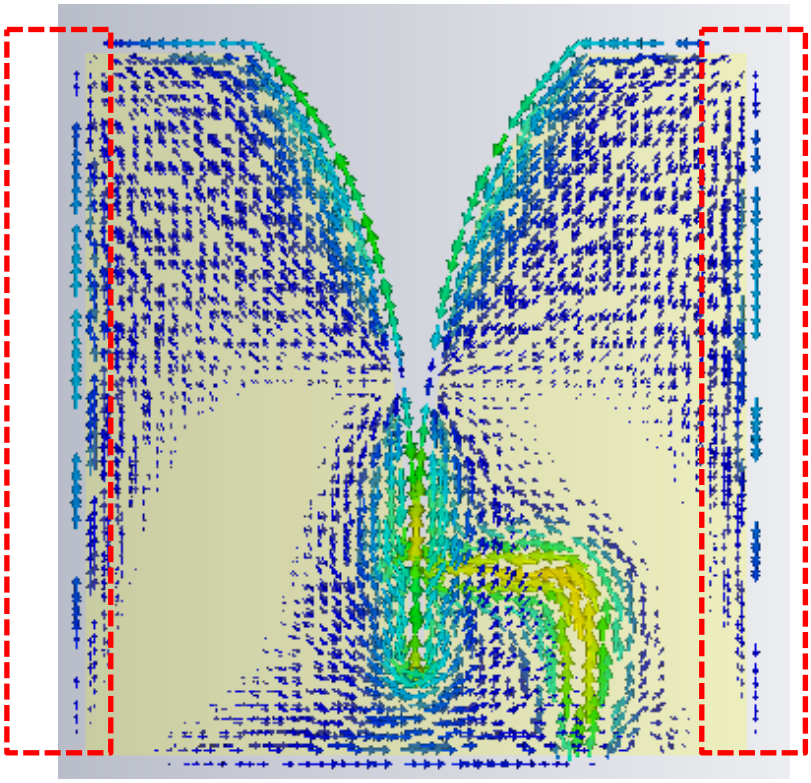

Figure 4.3: Current distribution of conventional Vivaldi antenna

along edge side is regarded as a dipole antenna, its radiation pattern is shown in Figure 4.4. With two currents flowing on left and right edge sides whose phase and amplitude are correlative, the backlobe of Vivaldi antenna is generated.

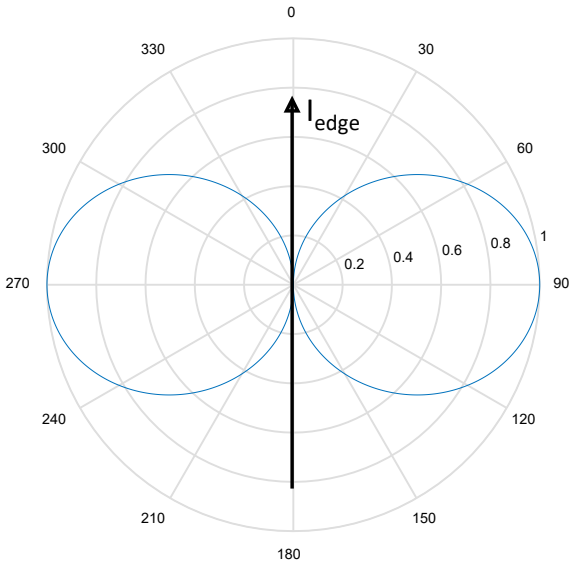

Figure 4.4: Radiation pattern of one-side current

In previous research [45], not only the mechanism of backlobe has been described, but also one single slit is inserted to edge sides to improve the FBR by changing current distribution. However, the position and length of slit has not been discussed.

In this section, a slit is inserted to edge sides to reduce the backlobe level and improve the FBR. Meanwhile, how the position and length of the inserted slit influence the backlobe level and gain will also be presented.

The layout of taper of Vivaldi antenna with single slit is shown in Figure 4.5. The feed line configuration is same as the conventional Vivaldi antenna. The width of slit is set to 3 mm which is much shorter than the wavelength.

As shown in Figure 4.5, parameter X and Y represents the position and length of inserted slit, respectively. By changing the X and Y, the simulated gain the FBR are shown in Figure 4.6(a), (b), respectively.

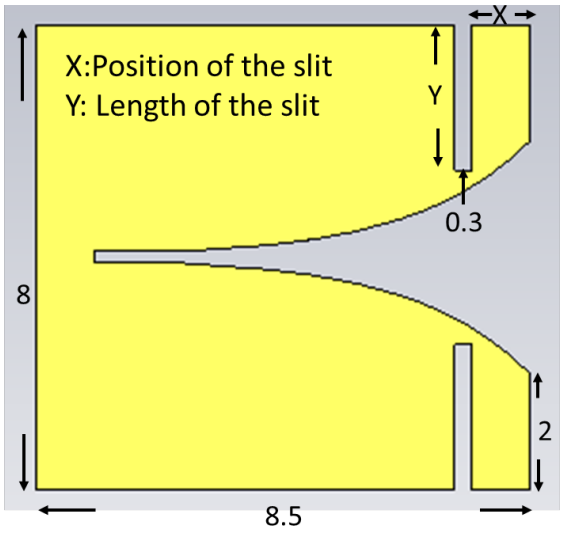

Figure 4.5: Layout of taper of Vivaldi antenna with single slit (Unit: mm)

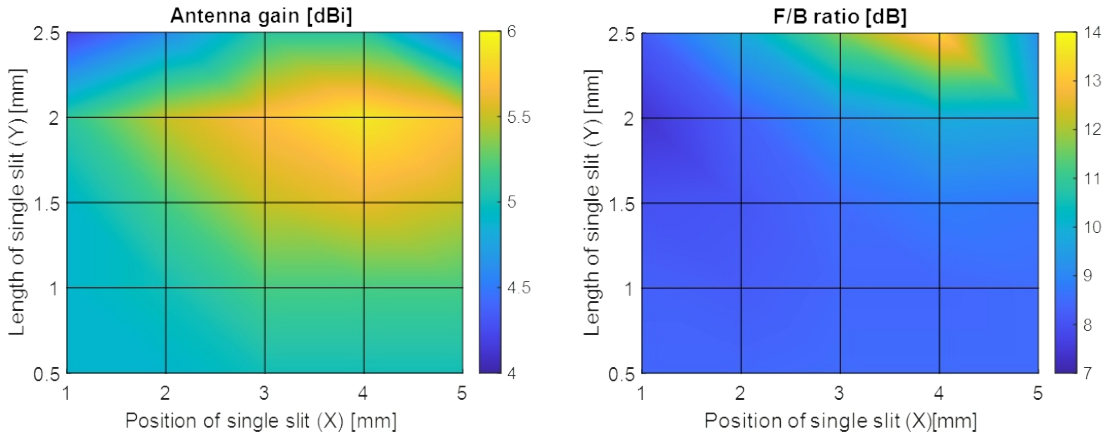

(a) Antenna gain (b) FBR

Figure 4.6: Simulation result of Vivaldi antenna with single slit

From Figure 4.6, it can be confirmed that, to achieve higher FBR, the position and length of corrugated slit shall be set around 3-4 mm and 2-2.5 mm, respectively. The position of single slit is around the middle of exponential taper where the current distribution is large as shown in Figure 4.3 and the length of single slit is around quarter of wavelength in the medium. The gain is almost unchanged. As a result, to achieve the best improvement on FBR, the single slit shall be inserted in where the current distribution is maximum and the length of single slit shall be set around quarter of wavelength to make open terminal on edge sides. So the current on edge sides can be minimized furthest.

The current distribution of Vivaldi antenna with single slit is shown in Figure 4.7. From Figure 4.7, it can be confirmed that the current on edge sides is reduced dramatically so that the FBR is improved furthest.

The simulation result of antenna gain pattern and reflection coefficient (S_{11}) of Vivaldi antenna (X=4 mm, Y=2.5 mm) with single slit is shown in Figure 4.8 (a), (b), respectively.

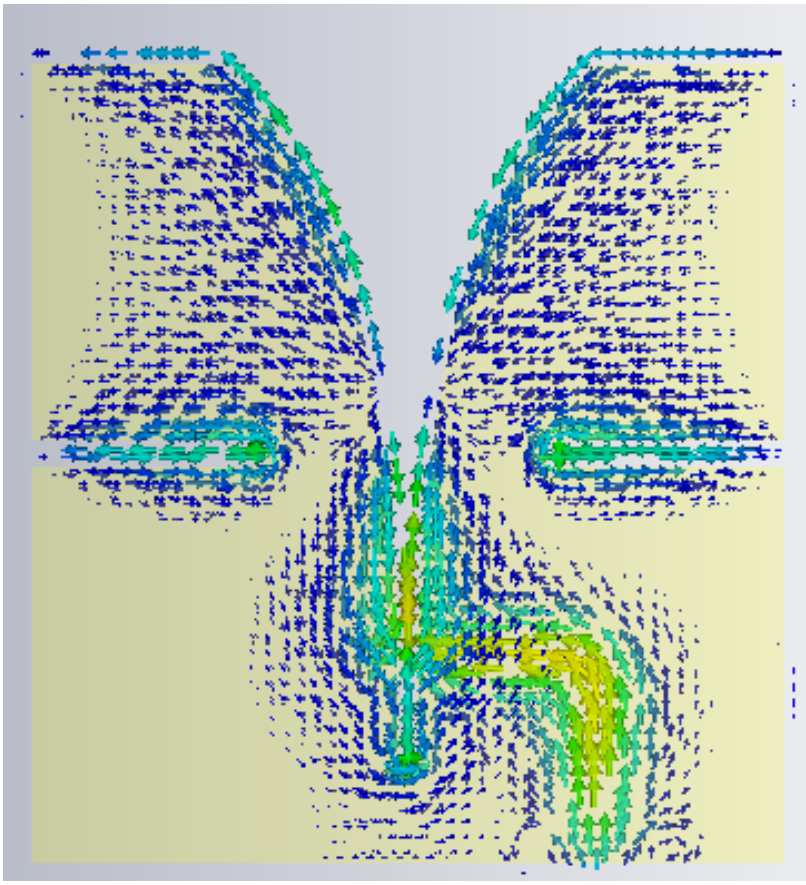

Figure 4.7: Current distribution of Vivaldi antenna with single slit

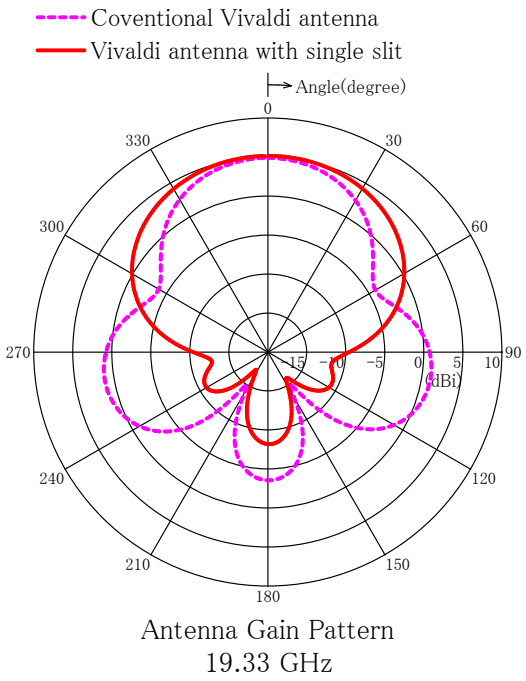

(a) Antenna gain pattern

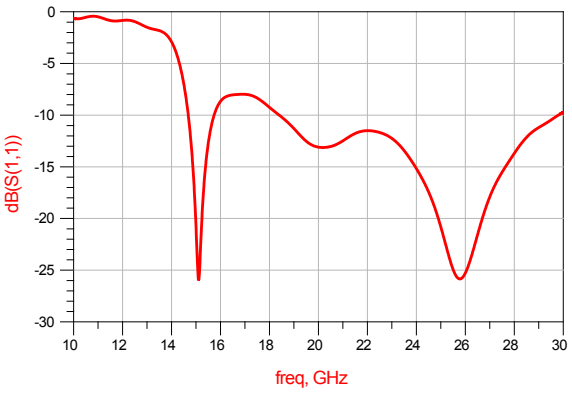

(b) S_{11}

Figure 4.8: Simulation result of Vivaldi antenna with single slit@X=4mm, Y=2.5mm

From Figure 4.8, it can be confirmed that the gain and backlobe level of Vivaldi antenna with single slit is 5.2 dBi and -8.2 dBi which means the FBR is 13.4 dB. Compared to the conventional Vivaldi antenna, the backlobe level decreased and FBR is improved. Around 20GHz band, the simulated S_{11} is below -10 dB.

4.3 Vivaldi antenna with two slits

To improve the FBR further, obviously, it is not sufficient using only single slit. In previous work [46–49], it has been demonstrated that using multiple inserted slit is a good method to improve FBR. However, as mentioned in previous section, without the investigation on the influence of position and length of inserted slit, a large number of slits is used.

In this section, Vivaldi antenna with two slits is proposed to improve FBR further, which has a simpler structure. Its layout is shown in Figure 4.9. The position and length of two slits is optimized by simulation and other parameters which are not shown are same as the conventional Vivaldi antenna.

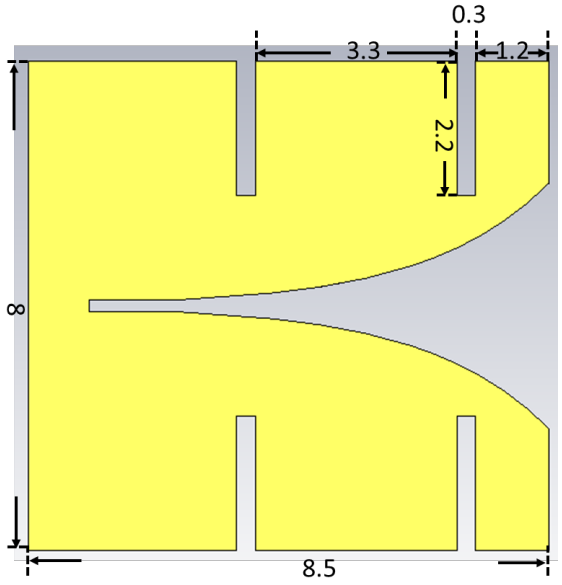

Figure 4.9: Layout of taper of Vivaldi antenna with two slit (Unit: mm)

The simulation result of antenna gain pattern and reflection coefficient (S_{11}) of Vivaldi antenna with two slits is shown in Figure 4.10(a), (b), respectively.

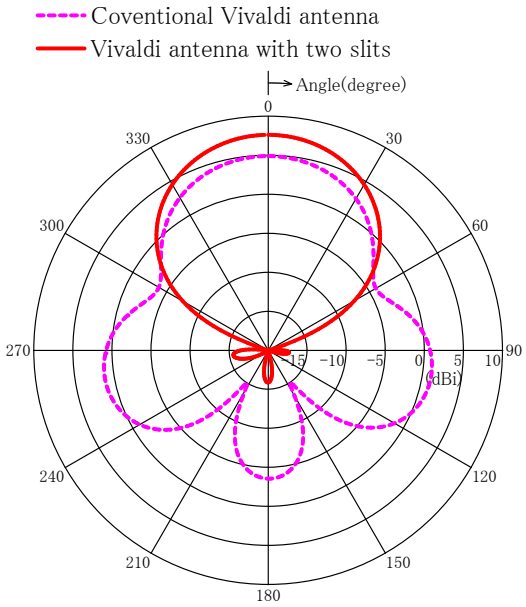

(a) Antenna gain pattern

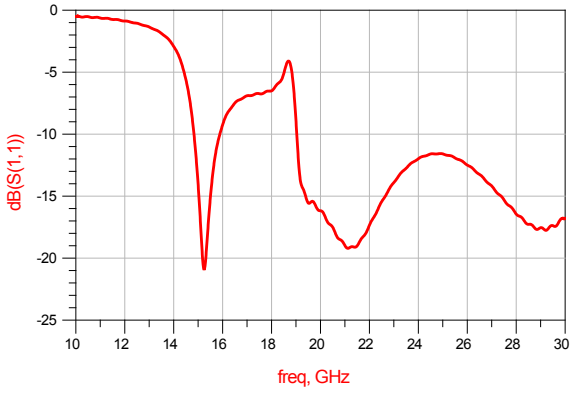

(b) S_{11}

Figure 4.10: Simulation result of Vivaldi antenna with two slits

From Figure 4.10, it can be confirmed that the gain and backlobe level of Vivaldi antenna with two slits is 7.6 dBi and -15.9 dBi which means the FBR is 23.5 dB. Compared to the Vivaldi antenna with single slit, FBR is improved further as expected. Take a further observation on the position and length of two inserted slits, the length is almost same as Vivaldi antenna with single slit and the position is symmetric by the position of single slit which is the middle of the exponential taper. It is because of the symmetric current distribution. Around 20GHz band, the simulated S_{11} is below -10 dB as well.

4.4 4-element Vivaldi array antenna based on two-slit configuration

4.4.1 Simulation result

The layout of 4-element Vivaldi array antenna based on two-slit configuration is shown in Figure 4.11, respectively.

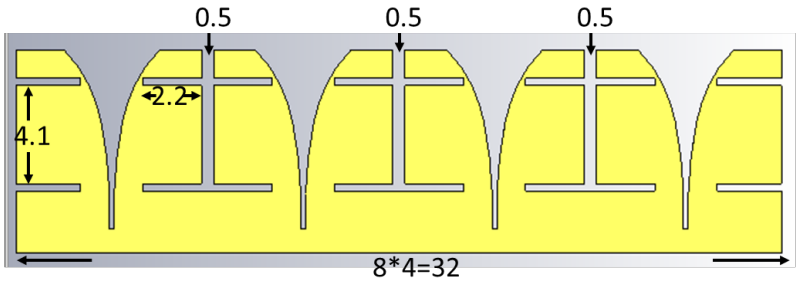

Figure 4.11: Layout of Vivaldi array antenna

The simulation result of antenna gain pattern and reflection coefficient (S_{11}) is shown in Figure 4.12(a), (b), respectively.

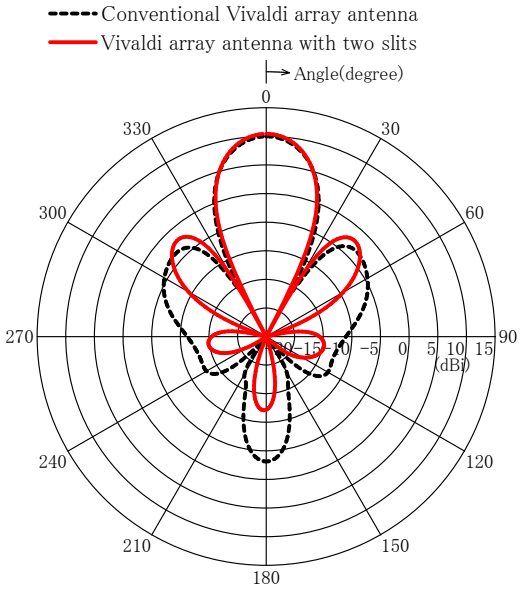

(a) Antenna gain pattern

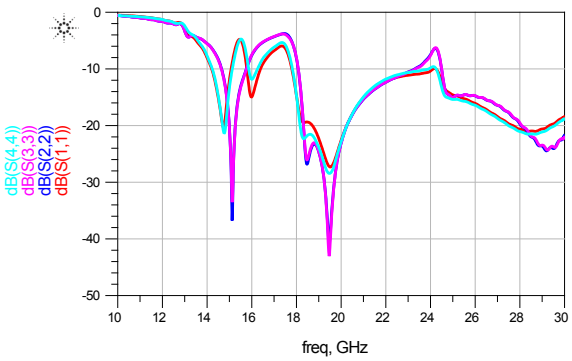

(b) S_{11}

Figure 4.12: Simulation result of Vivaldi array antenna based on two-slit configuration

It can be confirmed by simulation that the proposed Vivaldi array antenna has a good performance of reflection coefficient at 20GHz-band and its gain and backlobe level is 10.5 dBi and -15.1 dBi, resulting in an FBR of 22.6 dB which is very close to the simulation result of antenna element in the previous section.

Consequently, from the simulation result, the low-backlobe 4-element Vivaldi array antenna can be implemented by the proposed two-slit configuration.

4.4.2 Measurement result

The photo of fabricated 4-element Vivaldi array antenna is shown in Figure 4.13

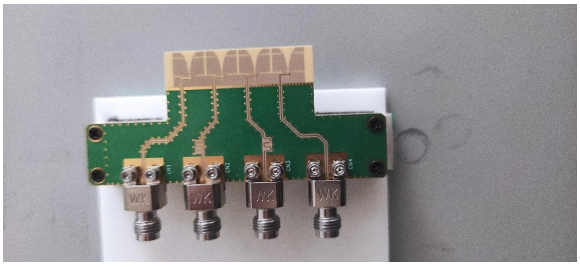

Figure 4.13: Photo of fabricated Vivaldi array antenna

The measurement result of reflection coefficient (S_{11}) is shown in Figure 4.14. The measured S_{11} of fabricated Vivaldi array antenna has a good performance of (S_{11}), as same as the simulation result.

The measurement result of antenna radiation pattern in inphase and quadrature phase of fabricated 4-element Vivaldi array antenna is shown in Figure 4.15(a), (b), respectively. As mentioned above, because of the limitation of measurement system, only front radiation pattern is measured. Despite this, the measured front radiation pattern still has a good agreement with simulation result. Therefore, the low-backlobe characteristics of the fabricated Vivaldi array antenna is expectable.

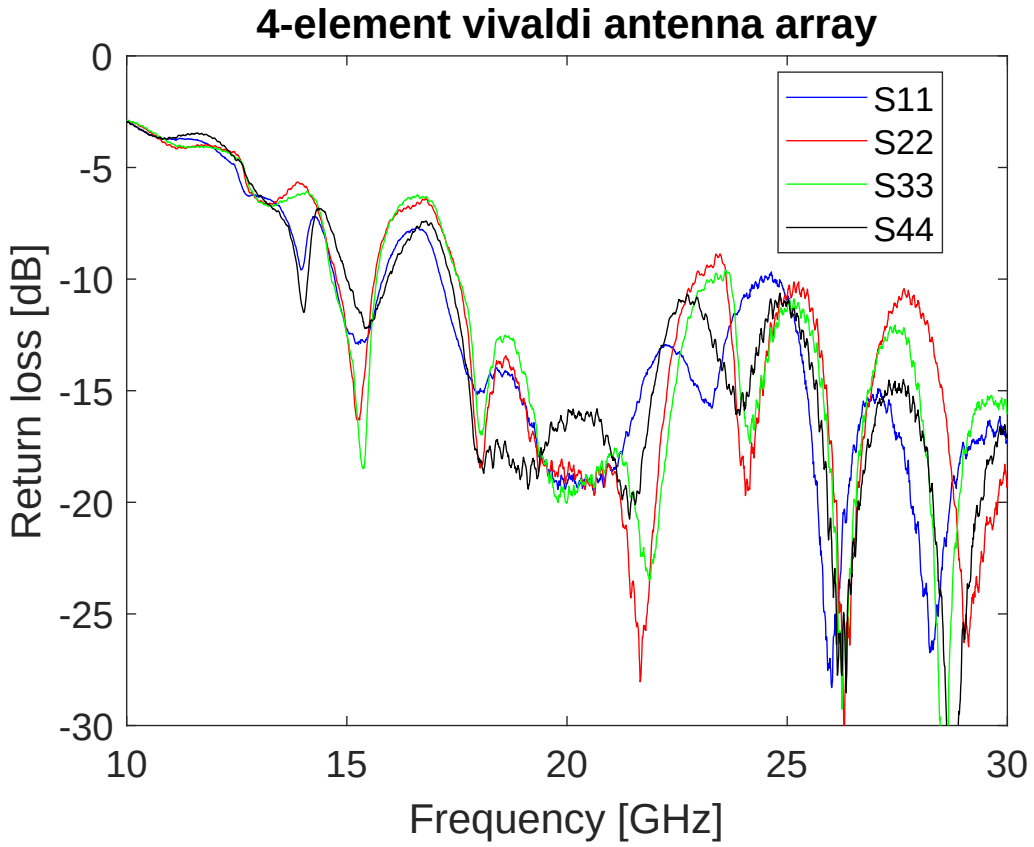

Figure 4.14: Measured S_{11} of fabricated Vivaldi array antenna

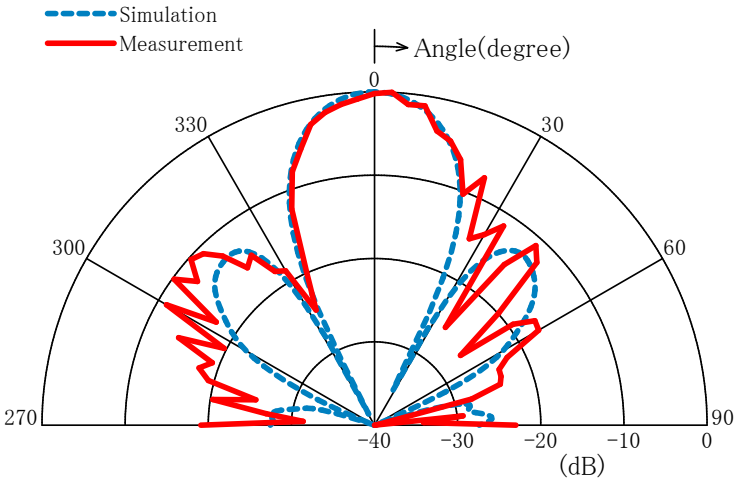

(a) Inphase

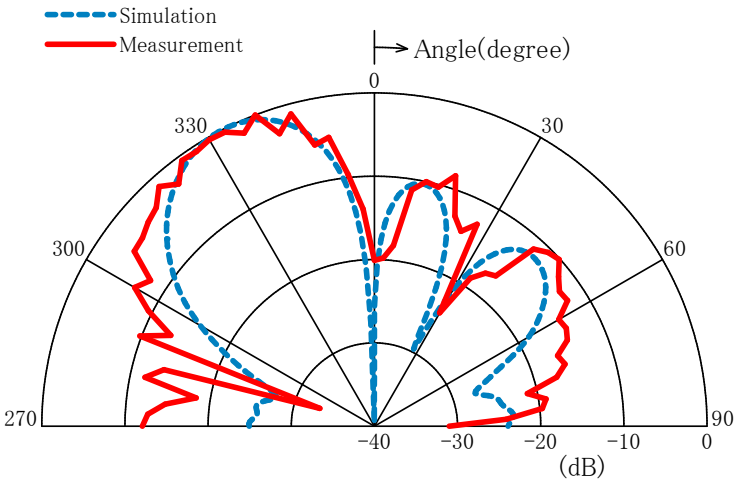

(b) Quadrature phase

Figure 4.15: Measured antenna radiation pattern of fabricated Vivaldi array antenna

4.5 Summary

In this chapter, first, to reduce the backlobe, Vivaldi antenna with single slit is simulated to investigate how the position and length of slit influence the backlobe. To improve the FBR further, two-slit configuration is proposed to reduce the current distribution on the edge sides which causes the high backlobe level. In simulation, it is proven that the proposed two-slit configuration is effective for both element antenna and array antenna that can improve the FBR to beyond 20 dB. To verify it, the 4-element Vivaldi array antenna based on two-slit configuration is fabricated and measured. Even though only front radiation pattern is measured because of the limitation of measurement system, the measurement result has a good agreement with the simulation result, which makes low-backlobe characteristics of the fabricated Vivaldi array antenna is expectable.

Chapter 5

Evaluation of the 20GHz-band DBF Transmitter Using Image Enhanced 1-Bit BP-DS Modulator

In this chapter, a 20GHz-band DBF transmitter using 1-bit BP-DS modulator implemented by the proposed image enhancement technique (chapter 2 and chapter 3) and 4-element low-backlobe Vivaldi array antenna is fabricated and evaluated (chapter 4).

5.1 Measurement result of the proposed image enhancement technique using Manchester coding and RF tripler at 20 GHz band

Since the frequency is normalized in the theoretical calculation, the effectiveness of proposed image enhancement technique using Manchester coding and RF tripler is irrelevant to frequency, which means it should be effective in any frequency band as well. To verify it, first, a simple transmitter module without antenna is fabricated as shown in Figure 5.1.

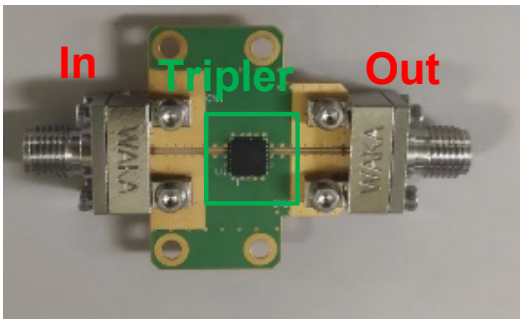

Figure 5.1: Photo of fabricated transmitter module

Only RF tripler (CY3-223+, Mini-circuit) whose input frequency is from 3.3 GHz to 7.3 GHz is implemented on module. The measurement set up is shown in Figure 5.2.

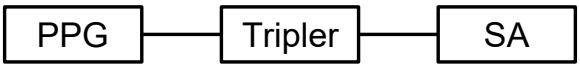

Figure 5.2: Measurement setup

In measurement, as well as chapter 4, the CW signal whose frequency is 1.501 GHz is modulated to 1-bit data by 1-bit BP-DS modulator whose sampling frequency is 6 GHz in MATLAB. Then, PPG (M18020A, Anritsu) is used to generate 1-bit signal in NRZ and Manchester code as the input of RF tripler. The amplitude is 1.3 V_{pp}, maximum value of PPG. The output signal is measured by spectrum analyzer(FSU67, R&S).

The measured input and output spectrums in NRZ and Manchester code condition are shown in Figure 5.3 and 5.4, respectively, with the RBW of 1 MHz.

At the first sight, it seems the 6^{th} order image component at 7^{th} Nyquist zone whose frequency is 19.501 GHz attenuates as output of RF tripler. However, it is not true. As mentioned above, the input frequency of RF tripler is from 3.3 GHz to 7.3 GHz. The 6^{th} order image component of 1-bit BP-DS modulated signal in Manchester code generated by PPG will be reflected, which means it can not be regarded as input signal of RF tripler.

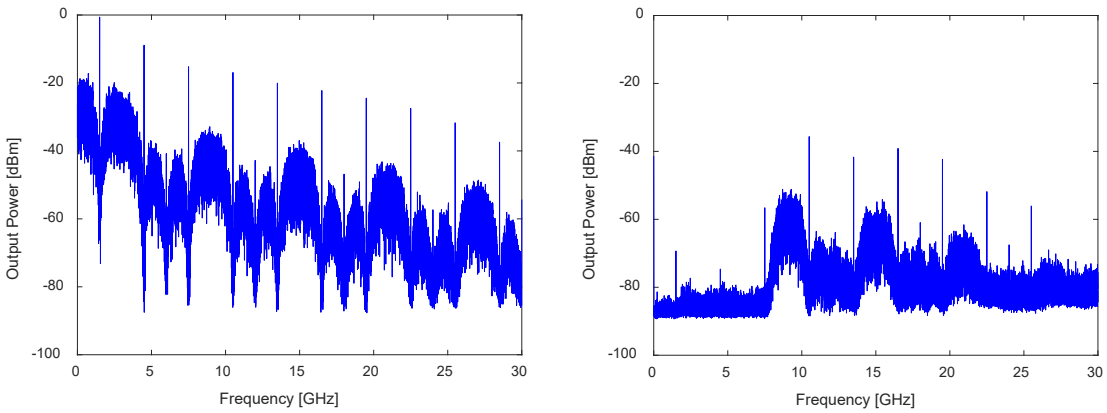

(a) Input spectrum (b) Output spectrum

Figure 5.3: Measurement result of RF tripler in NRZ code condition

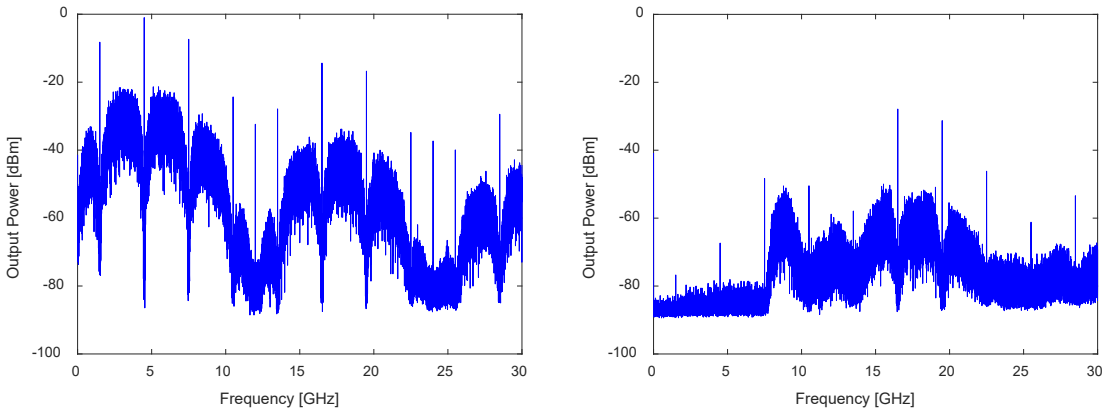

(a) Input spectrum (b) Output spectrum

Figure 5.4: Measurement result of RF tripler in Manchester code condition

To verify whether high order image component at 19.501 GHz is generated by RF tripler, the output amplitude of PPG is adjusted from 0.5 V_{pp} to 1.3 V_{pp}, step with 0.2 V. The output power of high order image component at 19.501 GHz is measured by SA with the RBW of 10 KHz, shown in Figure 5.5.

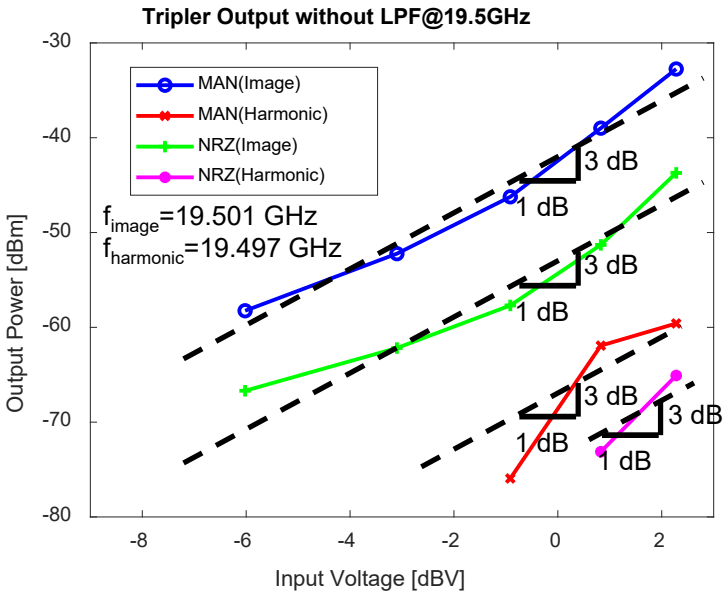

Figure 5.5: Output power vs. input voltage

From Figure 5.5, both the image and harmonic component of 1-bit BP-DS modulated signal in NRZ and Manchester code increase 3 dB when the input voltage increases 1 dB, which demonstrate that both the image and harmonic component are generated by RF tripler, not PPG.

The enlarged output spectrums at 19.5GHz-band in NRZ and Manchester code condition when the output voltage of PPG is set to 1.3 V_{pp} are shown in Figure 5.6(a), (b), respectively, with the RBW of 10 KHz.

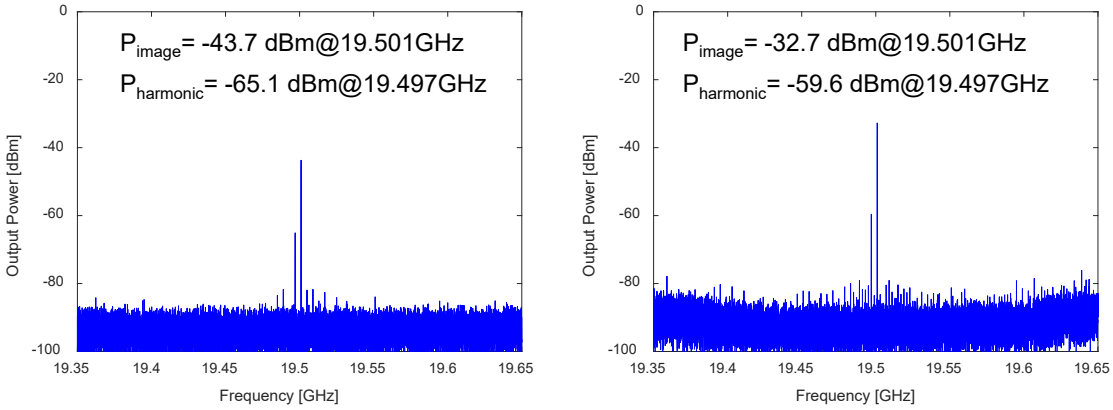

(a) In NRZ code condition

(b) In Manchester code condition

Figure 5.6: Enlarged output spectrums at 19.5GHz-band

In NRZ code condition, the output power of image and harmonic component are -43.7 dBm and -65.1 dBm, respectively.

In Manchester code condition, the output power of image and harmonic component are -32.7 dBm and -59.6 dBm, respectively, which means it has higher power and SNR, compared with NRZ code condition.

From the measured result, two significant findings described in chapter 2 and 3 have been proved in 20GHz-band. One is that the nonlinearity of the RF tripler enables the regeneration of high order image components. The other is that the regenerated high order image components exhibit superior performance in terms of output power and SNR in Manchester code condition rather than in NRZ code condition.

5.2 Evaluation of 4-element 20GHz-band DBF transmitter

5.2.1 Transmitter configuration

The overall transmitter configuration is shown in Figure 5.7. The RF tripler and 4-element Vivaldi array proposed in chapter 4 are integrated on one module. 1-bit BP-DS modulated signal in Manchester code is generated by PPG as the input signal of the fabricated module. The radiation pattern of proposed Vivaldi array antenna is measured in anechoic chamber. Only the front radiation pattern is measured, by step of 5°.

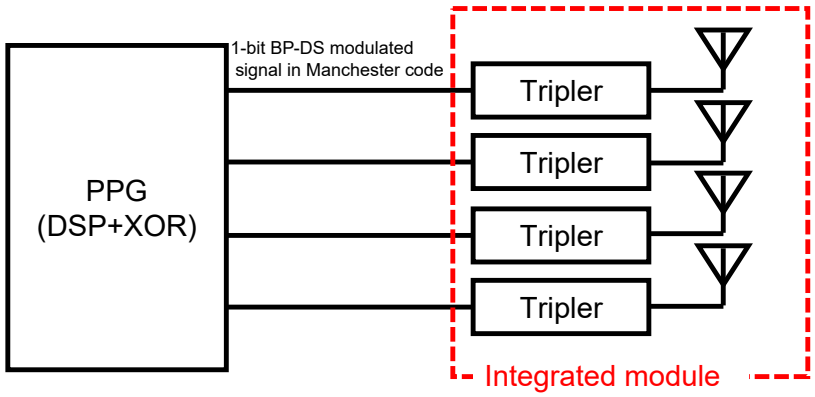

Figure 5.7: Overall transmitter configuration

5.2.2 Evaluation of element antenna

Before measuring the DBF transmitter, element antenna should be evaluated first. The measurement setup for evaluation of element antenna is shown in Figure 5.9

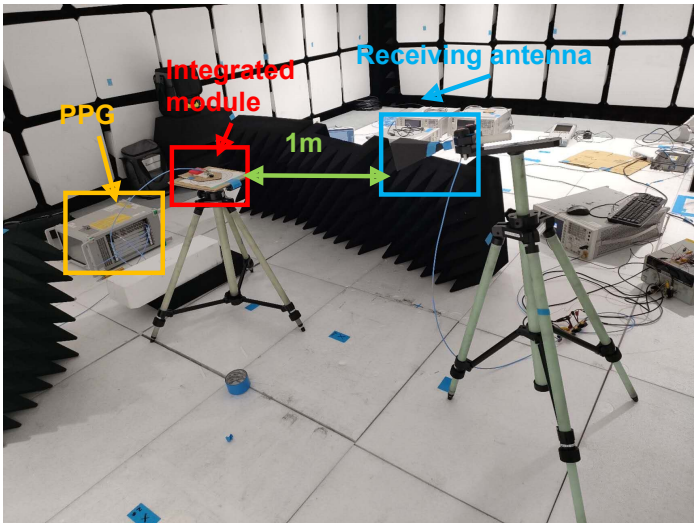

Figure 5.8: Measurement setup for evaluation of element antenna

The measured radiation pattern of element antenna is shown in Figure 5.9.

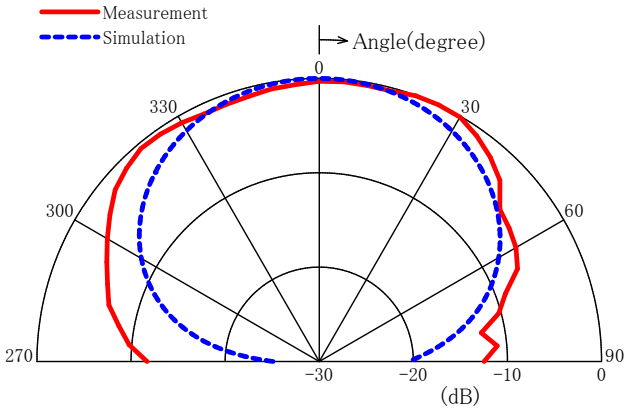

Figure 5.9: Measured radiation pattern of element antenna

Since the calibration of position and rotation of azimuth stage is conducted by manual, there must be some error in the measurement. Besides the mechanical instability, as mentioned above, the output power of RF tripler will increase/degrade by 3 dB as the input power increases/degrade 1 dB. The ripple (error) of input power of RF tripler will be tripled at output, which leads to the higher measurement error. Considering that, the measured radiation pattern of element antenna has a agreement with the simulation.

5.2.3 Evaluation of 4-element 20GHz-band DBF transmitter

The measurement setup for evaluation of 4-element 20GHz-band DBF transmitter is shown in Figure 5.10.

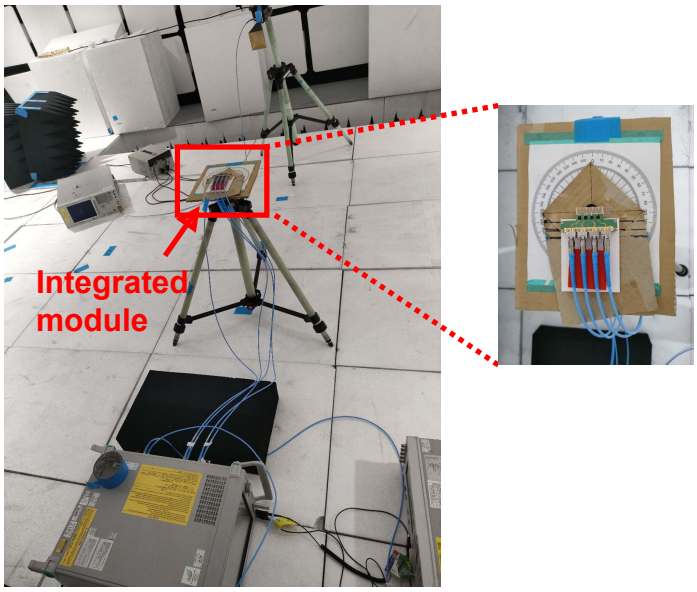

Figure 5.10: Measurement setup for evaluation of array antenna

The measured radiation pattern of 4-element 20GHz-band DBF transmitter in inphase and quadrature phase condition are shown in Figure 5.11(a), (b), (c), respectively.

As mentioned above in previous section, since all measurement of radiation pattern in this chapter is conducted by manual in addition with the nonlinearity of RF tripler, it is convincible that the measurement error is relatively large. Despite that, the beamforming characteristics can still be confirmed in the measurement result.

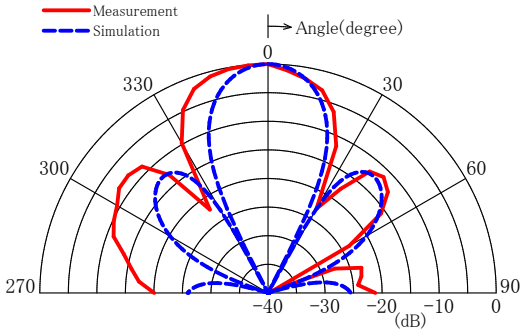

Antenna Radiation Pattern

(a) Inphase

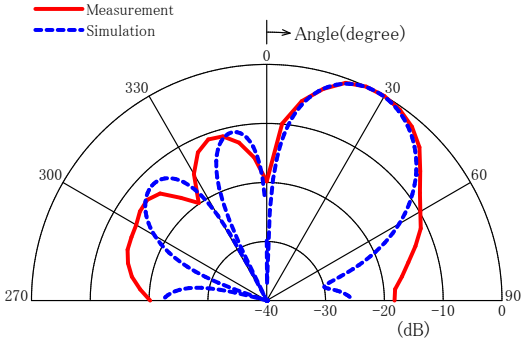

Antenna Radiation Pattern

(b) Quadrature phase (90°)

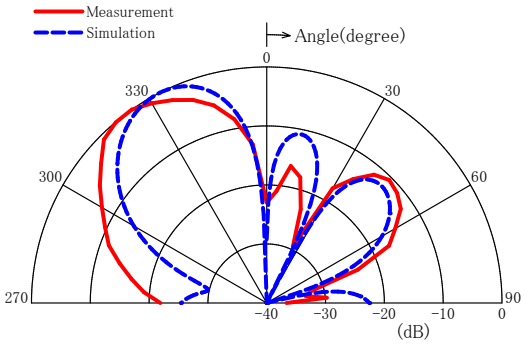

Antenna Radiation Pattern

(c) Quadrature phase (-90°)

Figure 5.11: Measured radiation pattern of 4-element 20GHz-band DBF transmitter

Chapter 6

Conclusions and Future Work

In this chapter, conclusion of this thesis will be presented followed by some proposals of future works.

6.1 Conclusion of this thesis

Nowadays, in the era of 5G/B5G, DBF transmitter in high frequency band can generate multiple beams simultaneously to realize the wireless communication in high speed and capacity. However, with the complex configuration, the miniaturization of transmitter module is necessary for practical implementation.

In the previous research, direct digital RF transmitter consisting of 1-bit BP-DS modulator using high order image components has been studied. Compared to the conventional transmitter, it can generate RF signal beyond the Nyquist limit and realize the miniaturization of transmitter by removing the mixer and LO so that it is applicable in the DBF transmitter. However, with the upper limit of sampling frequency of DSP which is 6 GHz, high attenuation for high order image components makes it difficult to generate RF signal in SHF band. The high attenuation is caused by the conventional NRZ coding scheme (digital domain) and the frequency characteristics of 1-bit DAC (analog domain).

To solve it, the image enhancement technique using Manchester coding (digital domain) and RF tripler (analog domain) is proposed and illustrated in chapter 2 and 3, respectively.

Meanwhile, the endfire antenna which can generate the beam horizontal to the substrate is preferable for its capability of integration with transmitter module. However, since its backlobe power will be reflected by metal transmitter module to frontward which influence the mainlobe, a shield is needed so that the complexity of transmitter is increased. It is not expected for miniaturization of transmitter.

So in chapter 4, a low-backlobe endfire Vivaldi array antenna is proposed and fabricated.

In chapter 2, image enhancement technique using Manchester coding in digital domain is described. It is confirmed by theoretical calculation, simulation and measurement that the high order image components of 1-bit BP-DS modulated signal in Manchester code at specific $(4n-1)^{th}$ and $(4n-2)^{th}$ Nyquist zone can be enhanced, compared with that in NRZ code. In the condition that the center frequency of 1-bit BP-DS modulator is quarter of sampling frequency, the improvement of the proposed image enhancement technique is 7.6 dB. The simulation result has a great agreement with calculation result, which proves the proposed image enhancement technique using Manchester coding in digital domain effective and feasible.

In chapter 3, image enhancement technique using RF tripler in analog domain is described. As mentioned above, the high order image components of 1-bit BP-DS modulated signal suffer a severe attenuation because of the frequency characteristics of 1-bir DAC. It is also confirmed by theoretical calculation, simulation and measurement that the attenuated high order image components can be regenerated or enhanced by RF tripler. Moreover, compared with the NRZ coding scheme, using Manchester coding can improve the output power of regenerated high order image components of 1-bit BP-DS modulated signal beyond 10 dB. Although there is some difference between the simulation and measurement, which may be caused by nonideal measurement device, the simulation and measurement results are still good evidence to prove the proposed image enhancement technique using RF tripler in analog domain effective and feasible and make it convincible that the high order image components can be regenerated by nonlinear device.

Since the frequency is normalized in the theoretical calculation, the effectiveness of proposed image enhancement technique using Manchester coding and RF tripler is irrelevant

to frequency, which means it should be effective in any frequency band as well.

In chapter 4, first, to reduce the backlobe, Vivaldi antenna with single slit is simulated to investigate how the position and length of slit influence the backlobe. To improve the FBR further, two-slit configuration is proposed to reduce the current distribution on the edge sides which causes the high backlobe level. In simulation, it is proven that the proposed two-slit configuration is effective for both element antenna and array antenna that can improve the FBR to beyond 20 dB. To verify it, the 4-element Vivaldi array antenna based on two-slit configuration is fabricated and measured. Even though only front radiation pattern is measured because of the limitation of measurement system, the measurement result has a good agreement with the simulation result, which makes low-backlobe characteristics of the fabricated Vivaldi array antenna is expectable.

In chapter 5, a 4-element 20GHz-band DBF transmitter using proposed image enhancement technique (chapter 2 and 3) and Vivaldi array antenna (chapter 4) is fabricated and evaluated. After it is confirmed that the RF tripler can regenerate the high order image components, radiation pattern of element antenna integrated with tripler into one module is measured. The measured radiation pattern has a agreement with simulation, considering that the measurement error is relatively larger because of the full manual measurement and RF tripler's nonlinearity. At the end of this chapter, a 4-element 20GHz-band DBF transmitter is evaluated. From its measured radiation pattern, the beamforming characteristics can be confirmed

In this thesis, to realize the miniaturization of DBF transmitter, 20GHz-band DBF transmitter using image enhanced 1-bit BP-DS modulator is proposed and the required elemental technologies of digital RF transmitter and antenna are developed and evaluated.

6.2 Future works

6.2.1 Modeling the nonlinearity of RF tripler more specificly

To illustrate the principle, in chapter 3, only two-tone signal are regarded as input signal of RF tripler. Although it can explain how the high order image components are regenerated, it is still a rough calculation because the noise and other low order image components have not been taken into the calculation, which leads to the difference between the calculation and simulation. Moreover, the operation of RF tripler is modelized as $y=x^3$ ideally without considering the device characteristics in practical implementation, which leads to the difference between the measurement and simulation.

Consequently, in future, not only the input signal but also the operation of RF tripler shall be modelized more specificly.

6.2.2 Evaluation of DBF transmitter

Although the 4-element 20GHz-band DBF transmitter using proposed image enhancement technique and Vivaldi array antenna has been evaluated in chapter 5, the measurement is completely conducted by manual, so the measurement result must be rough with the measurement error. The specialized jig and fixture may improve the measurement. Moreover, only single beam characteristics has been evaluated in the chapter 5. Multibeam characteristics of proposed 20GHz-band DBF transmitter should be evaluated in future as well.

Appendix A

List of Abbreviations

ADS Advances Design System

ACLR Adjacent Channel Leakage Ratio

ABF Analog Beam Forming

AMP Amplifier

BB Base Band

BP-DS Band Pass Delta-Sigma

BP-DSM Band Pass Delta-Sigma Modulator

BPF Band Pass Filter

B5G Beyond 5G

CMOS Complementary Metal-Oxide-Semiconductor

CW Continuous Wave

DBF Digital Beam Forming

DAC Digital-to-Analog Converter

DSP Digital Signal Processor

EHF Extremely High Frequency

FFT Fast Fourier Transform

FBR Front-to-Back Ratio

LO Local Oscillator

LPF Low Pass Filter

MOD Modulation

NRZ Non-Return-to-Zero

OSC Oscilloscope

PPG Pulse Pattern Generator

PSD Power Spectral Density

RBW Resolution Bandwidth

RF Radio Frequency

RZ Return-to-Zero

SHF Super High Frequency

SNR Signal-to-Noise Ratio

SA Spectrum Analyzer

TSA Tapered Slot Antenna

XOR Exclusive OR

Publications

Journal (with peer review)

[1] J. Zhang, M. Kazuno, M. Motoyoshi, S. Kameda, and N. Suematsu, ”Image Enhancement in 26GHz-Band 1-Bit Direct Digital RF Transmitter Using Manchester Coding,” *IEICE TRANSACTIONS on Communications*, Vol.E104-B, No. 6, pp. 654-663, 2021

[2] J. Zhang and N. Suematsu, ”Image Enhancement Technique Using Manchester coding and RF tripler for 1-Bit Bandpass Delta Sigma Direct Digital RF Transmitter,” *IEEE Access*, vol. 11, pp. 73359-73369, 2023

International conference (with peer review)

[1] J. Zhang, M. Kazuno, M. Motoyoshi, S. Kameda, and N. Suematsu, ”A 26GHz-band Image Enhancement Type 1-Bit DAC for Direct Digital 1-Bit Modulator,” *2018 Asia Pacific Microwave Conference (APMC2018)*, Kyoto, Japan, 2018, pp. 479-481

[2] J. Zhang and N. Suematsu, ”A 20GHz-Band Optical-Fiber-Feed 1-Bit Bandpass Delta-Sigma Direct Digital RF Transmitter Using First Image Component of the QSFP28 Module Output,” *2022 3rd URSI Atlantic and Asia Pacific Radio Science Meeting (AT-AP-RASC)*, Gran Canaria, Spain, 2022, pp. 1-4

[3] J. Zhang and N. Suematsu, ”40GHz-Band Direct Digital RF Modulator Using the 2nd Image Component of 1-Bit Delta-Sigma Modulated Signal,” *2022 Asia-Pacific Microwave Conference (APMC)*, Yokohama, Japan, 2022, pp. 496-498

[4] J. Zhang, K. Furuuchi and N. Suematsu, ”20GHz-Band Low Backlobe Vivaldi Endfire Antenna Array for Digital Beamforming Transmitter Antenna Module,” *2023 IEEE International Symposium on Radio-Frequency Integration Technology (RFIT)*, Cairns, Australia, 2023, accepted, waiting for publication

Domestic conference (without peer review)

[1] J. Zhang, M. Kazuno, M. Motoyoshi, S. Kameda, and N. Suematsu, ”A 26GHz-band Image Enhancement Type 1-Bit DAC for Direct Digital Transmitter,” *IEICE Technical Report MW2018-62*, vol. 118, no. 218, pp. 17-21, Sep., 2018

[2] J. Zhang, M. Kazuno, M. Motoyoshi, S. Kameda, and N. Suematsu, ”A 26GHz-band Image Enhancement Type 1-Bit DAC for Direct Digital Transmitter,” *IEICE Society Conference 2019*, C-2-88, Mar., 2019

[3] J. Zhang, M. Motoyoshi, S. Kameda, and N. Suematsu, ”Formulization for Output Power Spectral Density of 1Bit Direct Digital RF Transmitter Using Different Coding,” *IEICE General Conference 2021*, C-2-47, Mar., 2021

[4] J. Zhang and N. Suematsu, ”Image Signal Output Characteristics of Optical Fiber Feed Direct Digital RF Transmitter Using QSFP 28 Optical Module,” *IEICE General Conference 2022*, C-2-66, Mar., 2022

[5] J. Zhang and N. Suematsu, ”A 20GHz-Band Optical-Fiber-Feed 1-Bit BP-ΔΣ Direct Digital RF Transmitter Using First Image Component of the QSFP28 Module,” *IEICE Technical Report MW2022-44*, vol. 112, no. 118, pp. 66-71, Jul., 2022

[6] J. Zhang and N. Suematsu, ”40GHz-band Direct Digital RF Modulator using 2nd image component of 1-bit ΔΣ modulated signal,” *IEICE Society Conference 2022*, C-2-50, Aug., 2022

Bibliography

[1] NTT. ”technical journal for 5g”. [Online]. Available: https://www.docomo.ne.jp/binary/pdf/corporate/technology/rd/technicaljournal/bn/vol234/vol23_4_005jp.pdf

[2] W. Roh, J.-Y. Seol, J. Park, B. Lee, J. Lee, Y. Kim, J. Cho, K. Cheun, and F. Aryanfar, “Millimeter-wave beamforming as an enabling technology for 5g cellular communications: theoretical feasibility and prototype results,” *IEEE Communications Magazine*, vol. 52, no. 2, pp. 106–113, 2014.

[3] *Codebook-Based Beamforming Protocols for 5G Millimeter Wave Communications*.

[4] L. Guang, G. Wenbin, J. Boqi, L. Huijie, and Y. Jinpei, “Demonstration of a digital beamforming (DBF) transmitter array with 16 beams,” in *International Conference on Computational Problem-Solving*, 2010, pp. 82–84.

[5] T. Umezawa, P. T. Dat, K. Kashima, A. Kanno, N. Yamamoto, and T. Kawanishi, “100-GHz Radio and Power Over Fiber Transmission Through Multicore Fiber Using

Optical-to-Radio Converter," *Journal of Lightwave Technology*, vol. 36, no. 2, pp. 617–623, 2018.

[6] T. Nagayama, S. Akiba, T. Tomura, and J. Hirokawa, "Photonics-Based Millimeter-Wave Band Remote Beamforming of Array-Antenna Integrated With Photodiode Using Variable Optical Delay Line and Attenuator," *Journal of Lightwave Technology*, vol. 36, no. 19, pp. 4416–4422, 2018.

[7] B. Yang, Z. Yu, J. Lan, R. Zhang, J. Zhou, and W. Hong, "Digital Beamforming-Based Massive MIMO Transceiver for 5G Millimeter-Wave Communications," *IEEE Transactions on Microwave Theory and Techniques*, vol. 66, no. 7, pp. 3403–3418, 2018.

[8] M. Helaoui, S. Hatami, R. Negra, and F. M. Ghannouchi, *IEEE Transactions on Circuits and Systems II: Express Briefs, title=A Novel Architecture of Delta-Sigma Modulator Enabling All-Digital Multiband Multistandard RF Transmitters Design*, vol. 55, no. 11, pp. 1129–1133, 2008.

[9] M. S. Alavi, R. B. Staszewski, L. C. N. de Vreede, and J. R. Long, "A Wideband 2× 13-bit All-Digital I/Q RF-DAC," *IEEE Transactions on Microwave Theory and Techniques*, vol. 62, no. 4, pp. 732–752, 2014.

[10] M. S. Alavi, R. B. Staszewski, L. C. N. de Vreede, A. Visweswaran, and J. R. Long,

"All-Digital RF I/Q Modulator," *IEEE Transactions on Microwave Theory and Techniques*, vol. 60, no. 11, pp. 3513–3526, 2012.

[11] P. Cruise, C.-M. Hung, R. Staszewski, O. Eliezer, S. Rezeq, K. Maggio, and D. Leipold, "A digital-to-RF-amplitude converter for GSM/GPRS/EDGE in 90-nm digital CMOS," in *2005 IEEE Radio Frequency integrated Circuits (RFIC) Symposium - Digest of Papers*, 2005, pp. 21–24.

[12] J. Venkataraman and O. Collins, "An All-Digital Transmitter With a 1-Bit DAC," *IEEE Transactions on Communications*, vol. 55, no. 10, pp. 1951–1962, 2007.

[13] J. Keyzer, J. Hinrichs, A. Metzger, M. Iwamoto, I. Galton, and P. Asbeck, "Digital generation of RF signals for wireless communications with band-pass delta-sigma modulation," in *2001 IEEE MTT-S International Microwave Sympsoium Digest (Cat. No.01CH37157)*, vol. 3, 2001, pp. 2127–2130 vol.3.

[14] A. Jayaraman, P. Asbeck, K. Nary, S. Beccue, and K.-C. Wang, "Bandpass delta-sigma modulator with 800 MHz center frequency," in *GaAs IC Symposium. IEEE Gallium Arsenide Integrated Circuit Symposium. 19th Annual Technical Digest 1997*, 1997, pp. 95–98.

[15] T. Maehata, K. Totani, S. Kameda, and N. Suematsu, "Concurrent dual-band 1-bit digital transmitter using band-pass delta-sigma modulator," in *2013 European Microwave Integrated Circuit Conference*, 2013, pp. 552–555.

[16] T. Maehata, S. Kameda, and N. Suematsu, “A novel channel coding scheme for digital RF transmitter comprising a 1-bit band-pass delta-sigma modulator,” in *2014 Asia-Pacific Microwave Conference*, 2014, pp. 932–934.

[17] A. Agah, W. Wang, P. Asbeck, L. Larson, and J. Buckwalter, “A 42 to 47-GHz, 8-bit I/Q digital-to-RF converter with 21-dBm Psat and 16% PAE in 45-nm SOI CMOS,” in *2013 IEEE Radio Frequency Integrated Circuits Symposium (RFIC)*, 2013, pp. 249–252.

[18] Y. Zhou and J. Yuan, “A 1 GHz CMOS current-folded direct digital RF quadrature modulator,” in *2005 IEEE Radio Frequency integrated Circuits (RFIC) Symposium - Digest of Papers*, 2005, pp. 25–28.

[19] B. Jewett, J. Liu, and K. Poulton, “A 1.2GS/s 15b DAC for precision signal generation,” in *ISSCC. 2005 IEEE International Digest of Technical Papers. Solid-State Circuits Conference, 2005.*, 2005, pp. 110–587 Vol. 1.

[20] M.-J. Choe, K.-H. Baek, and M. Teshome, “A 1.6GS/s 12b return-to-zero GaAs RF DAC for multiple Nyquist operation,” in *ISSCC. 2005 IEEE International Digest of Technical Papers. Solid-State Circuits Conference, 2005.*, 2005, pp. 112–587 Vol. 1.

[21] N. Suematsu, “Direct Digital RF Technology - Challenges for Beyond Nyquist Frequency Range,” in *2018 IEEE International Symposium on Radio-Frequency Integration Technology (RFIT)*, 2018, pp. 1–3.

[22] R. Tamura, M. Motoyoshi, S. Kameda, and N. Suematsu, “7.5 GHz-Band Digital Beamforming Using 1-bit Direct Digital RF Transmitter with 10GbE Optical Module,” in *2021 51st European Microwave Conference (EuMC)*, 2022, pp. 51–54.

[23] M. Kazuno, M. Motoyoshi, S. Kameda, and N. Suematsu, “26 GHz-Band Direct Digital Signal Generation by a Manchester Coding 1-Bit Band-Pass Delta-Sigma Modulator using It’s 7th Nyquist Zone,” in *2018 11th Global Symposium on Millimeter Waves (GSMM)*, 2018, pp. 1–3.

[24] R. Tamura, M. Motoyoshi, S. Kameda, and N. Suematsu, “Output Signal Characteristics of Optical Fiber Feed Direct Digital RF Transmitter Using SFP+ Module,” in *2020 50th European Microwave Conference (EuMC)*, 2021, pp. 276–279.

[25] Karlupp. ”Microprocessor Trend Data”. [Online]. Available: https://github.com/karlrupp/microprocessor-trend-data

[26] Y. Yu, X. Zhang, J. Hu, and D. Huang, “All-optical clock recovery from both NRZ and NRZ-DPSK signals at different bit-rates,” in *2008 Conference on Lasers and Electro-Optics and 2008 Conference on Quantum Electronics and Laser Science*, 2008, pp. 1–2.

[27] D. Bishop, S. Million, T. Nguyen, and M. Simon, “Power spectrum of unbalanced NRZ and biphase signals in the presence of data asymmetry,” *IEEE Transactions on Electromagnetic Compatibility*, vol. 40, no. 1, pp. 55–61, 1998.

[28] J. Zhang and N. Suematsu, “40GHz-Band Direct Digital RF Modulator Using the 2nd Image Component of 1-Bit Delta-Sigma Modulated Signal,” in *2022 Asia-Pacific Microwave Conference (APMC)*, 2022, pp. 496–498.

[29] A. Frappe, A. Flament, B. Stefanelli, A. Kaiser, and A. Cathelin, “An All-Digital RF Signal Generator Using High-Speed $\Delta\Sigma$ modulators,” *IEEE Journal of Solid-State Circuits*, vol. 44, no. 10, pp. 2722–2732, 2009.

[30] J. Zhang and N. Suematsu, “A 20GHz-Band Optical-Fiber-Feed 1-Bit Bandpass Delta-Sigma Direct Digital RF Transmitter Using First Image Component of the QSFP28 Module Output,” in *2022 3rd URSI Atlantic and Asia Pacific Radio Science Meeting (AT-AP-RASC)*, 2022, pp. 1–4.

[31] A. Frappe, B. Stefanelli, A. Flament, A. Kaiser, and A. Cathelin, “A digital $\Delta\Sigma$ RF signal generator for mobile communication transmitters in 90nm CMOS,” in *2008 IEEE Radio Frequency Integrated Circuits Symposium*, 2008, pp. 13–16.

[32] J. Ala-Laurinaho, J. Aurinsalo, A. Karttunen, M. Kaunisto, A. Lamminen, J. Nurmiharju, A. V. Räisänen, J. Säily, and P. Wainio, “2-D Beam-Steerable Integrated Lens Antenna System for 5G E -Band Access and Backhaul,” *IEEE Transactions on Microwave Theory and Techniques*, vol. 64, no. 7, pp. 2244–2255, 2016.

[33] L. Wang, Y. Lian, and C.-H. Heng, “3–5 GHz 4-Channel UWB Beamforming Transmitter With 1° Scanning Resolution Through Calibrated Vernier Delay Line in 0.13-

μm CMOS," *IEEE Journal of Solid-State Circuits*, vol. 47, no. 12, pp. 3145–3159, 2012.

[34] S. Mondal, L. R. Carley, and J. Paramesh, "Dual-Band, Two-Layer Millimeter-Wave Transceiver for Hybrid MIMO Systems," *IEEE Journal of Solid-State Circuits*, vol. 57, no. 2, pp. 339–355, 2022.

[35] D. Schaubert, E. Kollberg, T. Korzeniowski, T. Thungren, J. Johansson, and K. Yngvesson, "Endfire tapered slot antennas on dielectric substrates," *IEEE Transactions on Antennas and Propagation*, vol. 33, no. 12, pp. 1392–1400, 1985.

[36] K. Yngvesson, T. Korzeniowski, Y.-S. Kim, E. Kollberg, and J. Johansson, "The tapered slot antenna-a new integrated element for millimeter-wave applications," *IEEE Transactions on Microwave Theory and Techniques*, vol. 37, no. 2, pp. 365–374, 1989.

[37] Y. Yu, W. Hong, Z. H. Jiang, H. Zhang, and C. Guo, "Multibeam Generation and Measurement of a DDS-Based Digital Beamforming Array Transmitter at Ka-Band," *IEEE Transactions on Antennas and Propagation*, vol. 67, no. 5, pp. 3030–3039, 2019.

[38] R. Forster, "Manchester encoding: opposing definitions resolved," *IET Engineering Science and Education Journal*, vol. 9, no. 6, pp. 278–280, 2020.

[39] G. K. Maity, S. P. Maity, and J. N. Roy, "All-optical Manchester code generator using TOAD-based D flip-flop," in *2012 International Conference on Devices, Circuits and Systems (ICDCS)*, 2012, pp. 479–481.

[40] M. Kazuno, M. Motoyoshi, S. Kameda, and N. Suematsu, “A study on the SNR in higher Nyquist zone of 1-bit low-pass delta-sigma RZ-DAC,” in *2017 IEEE Asia Pacific Microwave Conference (APMC)*, 2017, pp. 918–921.

[41] J. Zhang, M. Kazuno, M. Motoyoshi, S. Kameda, and N. Suematsu, “A 26GHz-Band Image Enhancement Type 1-Bit DAC for Direct Digital RF Modulator,” in *2018 Asia-Pacific Microwave Conference (APMC)*, 2018, pp. 479–481.

[42] Y. Zheng and C. E. Saavedra, “A Broadband CMOS Frequency Tripler Using a Third-Harmonic Enhanced Technique,” *IEEE Journal of Solid-State Circuits*, vol. 42, no. 10, pp. 2197–2203, 2007.

[43] C. Rauscher, “High-Frequency Doubler Operation of GaAs Field-Effect Transistors,” *IEEE Transactions on Microwave Theory and Techniques*, vol. 31, no. 6, pp. 462–473, 1983.

[44] S.-L. Jang, W.-C. Lai, Y.-J. Chang, D.-L. Wang, and M.-H. Juang, “CMOS Injection-Locked Frequency Quadrupler/Quintupler,” *IEEE Access*, vol. 10, pp. 78 168–78 175, 2022.

[45] Y. Xu, N.-W. Liu, and L. Zhu, “Proposal and design of an end-fire slot antenna with low back-lobe and improved front-to-back ratio,” *International Journal of RF and Microwave Computer-Aided Engineering*, vol. 31, no. 2, p. e22508, 2021.

[46] S. Choi, J. Ryu, and J. Lee, “Corrugated Tapered Slot Antenna with Band-stop Characteristic,” in *2020 IEEE International Symposium on Antennas and Propagation and North American Radio Science Meeting*, 2020, pp. 303–304.

[47] S. Sugawara, Y. Maita, K. Adachi, K. Mori, and K. Mizuno, “Characteristics of a MM-wave tapered slot antenna with corrugated edges,” in *1998 IEEE MTT-S International Microwave Symposium Digest (Cat. No.98CH36192)*, vol. 2, 1998, pp. 533–536 vol.2.

[48] M. Moosazadeh and S. Kharkovsky, “A Compact High-Gain and Front-to-Back Ratio Elliptically Tapered Antipodal Vivaldi Antenna With Trapezoid-Shaped Dielectric Lens,” *IEEE Antennas and Wireless Propagation Letters*, vol. 15, pp. 552–555, 2016.

[49] C. Fan, B. Wu, Y. Hu, Y. Zhao, and T. Su, “Millimeter-Wave Pattern Reconfigurable Vivaldi Antenna Using Tunable Resistor Based on Graphene,” *IEEE Transactions on Antennas and Propagation*, vol. 68, no. 6, pp. 4939–4943, 2020.

Acknowledgments

This research work took place in the Suematsu and Kameda Laboratory of Tohoku University. First and foremost I would like to express my deepest gratitude to my supervisor Prof. Noriharu Suematsu, who believed in me and took me under his guidance. Who constantly guided me and encouraged me throughout the course of the research work. Through his patience and instruction my mind has been opened and I have attained a deeper understanding of a broad spectrum of engineering principles.

My gratitude also goes to the other examining professors, Prof. Qiang Chen, Prof. Hiroki Nishiyama, and Prof. Suguru Kameda (Hiroshima University), for there critique and counsel without which this work would not be in this form.

I am also very grateful to Special Appointed Prof. Takashi Shiba, Special Appointed Prof. Satoshi Tsukamoto, Assoc. Prof. Mizuki Motoyoshi (Shizuoka Institute of Science and Technology) and Asst. Prof Tomoyuki Furuichi for their counsel and guidance which helped to mould and shape this work into its current state.

I would also like to acknowledge Visiting Assco. Prof. Takashi Maehata (Sumitomo Electric), I am grateful for the advice and counsel.

I would also like to thank Mr. Kazuyuki Totani (Direct RF) for the assistance of module fabrication.

I extend special thanks to Dr. Jean Temga (Silicon Austria Labs), Asst. Prof. Kohei Akimoto (Akita Prefectural University), Dr. Ahmad Abdalrazik (NICT Research Fellow), Mr. Takahiro Ono (Calsonic Kansei), Mr. Masafumi Kazuno (Murata Manufacturing), Mr. Yang Gui (Ericsson Japan), Mr. Kenta Mayama (NTT Communications), Mr. Nagahiro Yoshino (Mitsubishi Electric), Mr. Naoyuki Takeda (NHK), Mr. Kento Ono (KDDI), Mr. Taichi Yokouchi (NTT Communications), Mr. Xing Lv (Toshiba), Mr. Ryou Tamura (Murata Manufacturing), Mr. Koki Edamatsu (Mitsubishi Electric), Mr. Kei Yoshida (Hokkaido Electric Power), Mr. Bowen Dang (Toshiba), Mr. Syougo Takayama (Sigmaxyz), Mr. Daiki Machii (Sony Entertainment), Mr. Tsukasa Chida (Tokyo Electron), Mr. Takumi Aoki (MonoAI Technology), Mr. Yusaku Honma (Murata Manufacturing), Mr. Teru Ishimori (TDK) for their guidance and assistance, thank you for your willingness to offer assistance throughout my studies. I also offer special thanks to all the other students in the laboratory, Mr. Yuki Fujiya, Mr. Yuji Takatera, Mr. Koki Nakamura, Mr. Riku Ootomo, Mr. Fumito Karasawa, Mr. Esai Nagahari, Mr. Koki Furuuchi, Mr. Fumiaki Wakiya, Mr. Ryunosuke Saito, Mr. Eito Sato, and Mr. Tomoki Nakazawa.

I would like to thank Ms. Yukie Tomizawa, Ms. Kaori Yamada and Ms. Kaori Toshi for their support and assistance in handling all the necessary paper work.

I would like to thank AIE-WISE Program and Support for Pioneering Research Initiated by the Next Generation for their financial support and internship opportunity.

My deepest gratitude goes to my family and all my friends who encouraged and supported me during my studies. Without them this work would never have been possible. From the bottom of my heart I thank you all.

I also thank everybody else who I haven't mentioned here who may have contributed to my research.